Towards Development of Indigenous Differential Spectroscopic Instruments

A thesis by

Dhairya Bhandari

towards the partial fulfillment of the BS-MS dual degree, under the supervision of

Dr. Ashish Arora

Department of Physics
Indian Institute of Science Education and Research, Pune

Certificate

This is to certify that this dissertation entitled "Towards Development of Indigenous Differential Spectroscopic Instruments" towards the partial fulfilment of the BS-MS dual degree programme at the Indian Institute of Science Education and Research, Pune represents study/-work carried out by Dhairya Bhandari under the supervision of Dr. Ashish Arora, Assistant Professor, Dept. of Physics, Indian Institute of Science Education and Research, Pune during the academic year 2025-2026.

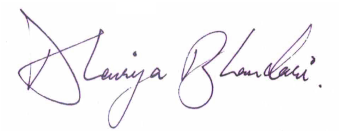

Dhairya Bhandari

Dr. Ashish Arora
Assistant Professor
IISER Pune

Declaration

I hereby declare that the matter embodied in the report entitled "Towards Development of Indigenous Differential Spectroscopic Instruments" are the results of the work carried out by me at the Department of Physics, Indian Institute of Science Education and Research, Pune, under the supervision of Dr. Ashish Arora and the same has not been submitted elsewhere for any other degree.

Dhairya Bhandari

Dr. Ashish Arora
Assistant Professor
IISER Pune

Statement of AI Usage

I hereby declare that no artificial intelligence/large language models were used in the production of the report entitled “Towards Development of Indigenous Differential Spectroscopic Instruments”

To the instruments that made this thesis possible,
& the instruments that this thesis makes possible.
The instruments that gave up their life in my hands,
& the instruments my hands gave life to.

Acknowledgements

This thesis marks one of the final chapters of my time at IISER. This will remain, perhaps, one of the most formative parts of my life. Any such saga, for that is the only word I can think of that appropriately describes what happened in the five years I spent here, is incomplete without an ensemble cast, and this one is no exception. Before I thank all of them, I must ask the forgiveness of those who I will have missed but not forgotten, for one can only say so much in such few pages, and my memory fails me far too often.

First of all, I thank my supervisor, Dr. Ashish Arora. His emphasis on regular chai breaks have been the nudge that pushed me through many of the pivotal moments of this thesis. His less regular, but more insightful dispensation of advice has contributed substantially to my growth as a student, not only of physics, but also of the more imposing university of life. His candour and cheerfulness are what made this lab an absolute pleasure to work in. I must also blame him for the death of my sense of humour, which he has ruined completely with his terrible puns that any who have spoken to him would recall.

I also thank Prof. Seema Sharma, Prof. Arnab Bhattacharya, Dr. Shouvik Chatterjee, and Prof. Bhas Bapat, who took a chance on me when I was a young student. They are responsible for introducing me to the fascinating world of experimental physics, which I fell in love with instantly. Prof. Shivprasad Patil helped me extend this love to the intricate world of electronics. He has also suggested some superb novels, that were a wonderful way to take the stress off of the mind at the end of the day.

I would also like to thank the National Quantum Mission and the Kishore Vaigyanik Protsahan Yojana for their generous support. I would also like to point out that the Kishore Vaigyanik Protsahan Yojana was the turning point in my life which made it abundantly clear to me that I wanted to do science. I deeply mourn its discontinuation.

My colleagues at the High Precision Magneto-Optics Lab have been instrumental in the completion of their thesis, and I would be nowhere without their continued support. I must first thank Gautam, Riyanka and Sayantan, with whom I have spent countless days, and the odd nights in between, working on designs and experiments. I would also like to thank Vinod and Ranjuna, who's advice was what has led me to rebut the results of one particularly popular experiment[1]. The camaraderie of Sourabh, Aditi, Arundhati, Piyush, Aparna, Rayees, Bhumika and Abhisek is what makes the student room of the lab such a pleasant environment. I would also like to thank my former colleagues in the Quantum Materials Lab at the Tata Institute of Fundamental Research, especially Shikhar, Nileshji and Devendraji, for being founts of wisdom and advice during my time there in my earlier years.

I also extend my gratitude to the various clubs of IISER Pune, for taking my sweat and blood, and never complaining when they fell short. Mīmāṃsā, which is not a quiz, has been one of the most exhilarating experiences I have been a part of, whether as a photographer or

[1] Upper, D. (1974), The Unsuccessful Self-Treatment of a Case of "Writer's Block". Journal of Applied Behavior Analysis, 7: 497-497

as part of the Physics question making team. But this is only because of the people I have met here, such as Mogra, Soumil, Sugat, Dhruv, Dipansh, Harshal, Soumya, Nachiketa, Eeshaan, and various others. The Bookworms Library, tucked away in Hostel 1, and then Hostel 2 was a wonderful way to regularly waste Sunday afternoons which meeting readers, and sharing recommendations. Once again, it is the people that made it the special place it is. Shree Hari, Vasudha, Krish, and Basudha come to mind.

My many friends on this campus have both kept me going, and kept me from going insane. Ahan, Kartik, Kāvyā, and Mogra have been there for me, even when I wasn't there for myself. Das, Krishna, Sanskruti, Ameya, Moksh, have all kept me company through rain and shine. The various board gamers on campus, Kāvyā, Srirang, Paritosh, Seona, and many others, have always been excellent folk to battle wits with. Beyond my own batch, Vikram Iyer, Akash Dutta, Parijat, Shreya, Sana, Nakul, Vinayak, Aaditya Datar, Lokesh Venkatesh, and many more who I am sure I am forgetting, have been wonderful people to keep bumping into.

My friends and family from beyond the campus have been pillars of support, despite the distance between us. Long calls with Anjika, Pranav, and Shruti have been crucial escapades from the travails that IISER puts one through. Bharat nanu and Lalit dadu have been most encouraging mentors, not only in pursuing science, but also in fulfilling my hobbies, particularly photography. Shriya has always been a delight to talk to.

My parents, I must thank for imbuing me with the scientific temper that has carried me here, and on whose wings I continue to fly[2]. Their love has allowed me into blossom into the person that I am today.

I would also like to mention the devices that have supported me through this thesis. My loyal laptop, LapTrap, who has been my comfort machine. My D3000 and D5600, with whom I can photograph blindfolded. My wonderful headphones, that have kept distraction at bay during critical moments. Also, the few cafes around IISER, in particular, Pagdandi, Aeka, Comics and Brics, and Demitasse, have been warm and cozy hideouts for when the caffeine ran low, and the morale ran lower. They have been excellent all weather morale boosters.

[2] *The Nights* by Avicii always reminds me of what my father told me of resistors

Contents

List of Figures

List of Tables

Abstract

Layered 2D semiconductors and magnets demonstrate novel excitonic physics. Their magnetic properties can be effectively studied at low fields using differential spectroscopy techniques such as Faraday effect and magneto-optic Kerr effect. The precision of these techniques can be further improved by the use of the Sagnac effect, which is only sensitive to magnetic effects. In this thesis, a broadband magneto-optic Kerr effect measurement technique, based on the Sagnac effect, is proposed on the basis of Jones matrix analysis. Its assembly and testing procedure is described. An effective technique to characterise candidate samples for Kerr spectroscopy is scanning photoluminescence microscopy. Improvements to the speed and resolution of an existing scanning photoluminescence microscope, used to characterise monolayer semiconductors are presented. Photoluminescence scans of tungsten disulphide flakes, highlighting monolayer regions, are demonstrated. In order to carry out these magneto-optic measurements over a wide spectral range, broadband LED light sources, and compact magnetometers are highly desirable. The design and construction of a broadband LED source, with emission from 400 nm to 1000 nm, is described. Its suitability for spectroscopic measurements, in terms of stability, is shown. Additionally, the design and construction of a compact, cost-efficient 0 T to 0.5 T magnetometer, and its interfacing with SCPI, is presented.

Chapter 1

Introduction

Optical spectroscopy is a powerful and versatile tool, that is essential to understanding the electronic and optical behaviour of condensed matter systems. The understanding of how light and matter interact can provide insight into electronic properties, such as band structure shifts, excitonic effects, and electronic phase transitions, in semiconductors. Differential spectroscopy is an optical technique that has gained popularity recently, as it can sense very minute shifts in band structure, caused by external perturbations such as applied magnetic fields, or changing temperature.

Differential spectroscopy compares the optical properties of a material for two orthogonal polarisations, in order to extract very precise information about shifts in band structure. An excellent set of examples are the magneto-optic Faraday and Kerr effect.[1, 2] In the Faraday effect, a plane polarised beam of light is rotated as it travels through a magnetised material.[3] In the Kerr effect, rotation occurs upon reflection from a magnetised surface.[4] Measuring the degree of rotation as a function of wavelength provides valuable information about the electronic spins in a material.[1, 5] In particular, these magneto-optical techniques can be used to extract parameters such as the g-factor of exciton lines in semiconductors, even under relatively small magnetic fields. [5, 6].

The Sagnac interferometer has been proposed as a technique to sense these effects with μrad precision.[7] This interferometer works by sending two beams of light along the same circular path, in opposite directions. Upon recombining, they produce interference that is dependent only on effects that depend on the direction of travel, as the physical path for both the beams is the same.[8] Magneto-optical effects, that depend on the direction of light relative to the magnetic field, are an example of such effects, making the Sagnac interferometer uniquely suited to measuring them.

Despite their advantages, conventional Sagnac interferometry based magneto-optic instruments are limited in bandwidth over which they can measure Kerr or Faraday effects, to approximately 22 nm.[9] This is due to the use of polarisation-maintaining optical fibres and photoelastic modulators.[7, 10, 9] These instruments have suitable polarising properties only over a narrow region of the visible-infrared spectrum[11]. Moreover, the use of photoelastic modulators limits the speed at which a spectral sweep can be done[11].

Consequently, the development of broadband Sagnac interferometry instruments capable of performing rapid, spectrally resolved magneto-optical measurements, is an important experimental challenge. Assembling such high-precision spectroscopes also requires high precision opto-mechanical and opto-electronic components. India has the hidden capability to produce such precise components, but remains dependent on international suppliers such as ThorLabs, Edmund Optics and Newport to fulfil her requirements for such components.

To overcome these challenges, we propose the design of a broadband Sagnac interferometer to measure Kerr rotation and Kerr ellipticity spectra. This design is capable of simultaneous measurement over the wavelength range of 500 nm to 800 nm. Along with this, the development of indigenously built high precision opto-mechanical and opto-electronic components is discussed.

In addition to the Sagnac interferometer, this thesis also presents work done towards the development of a scanning photoluminescence imaging confocal microscope. This instrument combines micron-scale spacially resolved imaging with spectral analysis, enabling rapid characterisation of the optical characteristics of layered two dimensional semiconductors, and van der Waals heterostructures.

1.1 Differential Spectroscopy

As previously noted, differential spectroscopy senses the change in the polarisation state of light, when it interacts with the sample. This change in polarisation occurs due to the sample having different complex refractive indices for light of different polarisation[1]. The polarisation state of light can always be described as a superposition of two basis polarisation states.[12, 13, 14] There are two such bases in which this difference in refractive index is easy to intuitively understand[12], as illustrated in Table 1.1.

Name of Basis	Eigenvectors	Illustration
Linear	$\begin{bmatrix}1\\0\end{bmatrix}$	
	$\begin{bmatrix}0\\1\end{bmatrix}$	
Circular	$\begin{bmatrix}1\\i\end{bmatrix}$	
	$\begin{bmatrix}1\\-i\end{bmatrix}$	

Table 1.1: Commonly Used Polarisation Eigenbases[2, 12]

When the real part of the refractive index is different for two polarisation states, it is known as birefringence, and when the imaginary part is different, it is known as dichroism[12, 14]. Circular birefringence leads to the rotation of plane polarised light, whereas circular dichroism leads to ellipticity, i.e., the field vector of the light beam traces an ellipse as it propagates. On the other basis, linear birefringence causes ellipticity, whereas linear dichroism causes rotation.[1, 2, 12, 14]

These effects are further classified on the basis of the geometry in which they are detected and their dependence on the applied magnetic field. There are two main geometries; the Faraday geometry, in which the magnetic field is parallel to the propagation of light; and the Voigt geometry, in which the magnetic field is perpendicular to the propagation of light.[15]. In transmission, the rotation of a plane polarised beam light is known as the Faraday effect, and the ellipticisation is known as magneto-circular dichroism.[15]. In reflection, these effects are known as Kerr rotation and Kerr ellipticity.[15]

These effects are extremely strong near the exciton lines of a semiconductor.[1, 5, 15] Hence, they can be used to understand how the bands shift under the influence of a magnetic field, even at fields as low as 1 T. This provides further insight into the band structure of a semiconductor, such as the spin-resolved nature of the bands.[5]

Sagnac interferometry offers a uniquely precise way to measure such magneto-optic effects, due to its inherent insensitivity to effects that obey time-reversal symmetry, as discussed in Section 1.2.

1.2 Sagnac Interferometry

A Sagnac interferometer is a device that is sensitive only to changes that break time-reversal symmetry, encoding them into a change in light intensity.[12, 13] A schematic is shown in Figure 1.1.

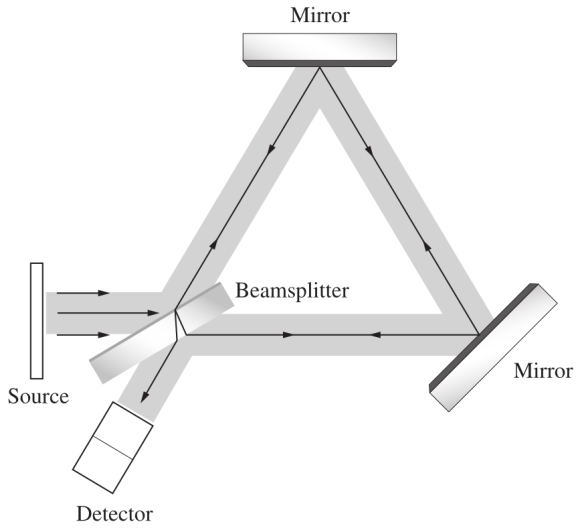

Figure 1.1: Optical Schematic of a Sagnac Interferometer[12].

Suppose that the instrument shown in Figure 1.1 is rotating clockwise with a constant angular velocity. Hence, for the light beam travelling anticlockwise, the length of the loop back to the beamsplitter will appear shorter, as compared to that for the beam travelling clockwise. As a result, the two beams have a path difference, and a corresponding phase difference. This phase difference is known as the Sagnac effect.[12] It can be measured, as a dip in intensity, and can be used to measure the speed of rotation of the apparatus.[8, 12, 13]

It is important to note, that since both beams take the same physical path, they both suffer the same phase shifts from elements such as mirrors, beam splitters, lenses, and any other non-magnetic element in the loop. Hence, they provide very precise measurements of angular velocity, provided the geometry is known.[7]

This ability of the Sagnac interferometer to sensitively measure rotation has been used extensively in developing gyroscopes.[16]. However, such a phase shift can also be produced by magneto-optic effects.[1] There are various reports of Sagnac interferometers that measure both Kerr and Faraday rotation.[7, 9, 10] Extensive work has been done by the group of Aharanov Kapitulnik *et al.* in developing these techniques, and applying them to study the superconducting phase transition under the influence of a magnetic field.[17] There are

also reports of using Sagnac interferometers to measure time-resolved magneto-optic Kerr effect[18, 19].

In order to carry out broadband Sagnac interferometric Kerr effect measurements on 2D layered semiconductor materials, two things are desirable. First are high quality samples to carry out measurements on, and second, are compact, efficient, broadband light sources, and magnetometers.

Transition metal dichalcogenides possess sharp excitonic features, characterised by large exciton binding energies[20], strong oscillator strengths[21], and large g-factors[22], that arise from their confined nature. This makes them an ideal material system for Sagnac spectroscopy[23]. TMDCs can be efficiently characterised by a scanning photoluminescence microscope described in Section 1.3. A broadband light source and a magnetometer, is described in Section 1.4.

1.3 Scanning Photoluminescence Microscopy

Spacially-resolved photoluminescence spectroscopy is essential to the rapid characterisation of layered two-dimensional materials. For example, the photoluminescence spectra of monolayer transition metal-dichalcogenides (TMDCs) is visibly distinct from that of bilayer or thicker TMDCs.[24] This enables easy identification of monolayer flakes. A confocal scanning photoluminescence microscopy, which can provide such spacially resolved photoluminescence maps is an ideal technique for such characterisation.

This thesis builds upon prior work done on such a confocal laser scanning microscope[25], which uses galvanometer-mounted mirrors (galvo mirrors) to precisely steer the incident light beam, allowing an automated scan of the sample. It also uses a temperature compensated avalanche photodiode (APD) to detect photoluminescence from the sample, and can thus create photoluminescence scans of van der Waals heterostructures. In this thesis, the electronic control of the galvo mirrors and synchronisation with the APD is improved, and a spectrometer is coupled in order to construct photoluminescence images of samples.

A schematic of the optical system is shown below in Figure 1.2. The mirror shown is mounted on a galvanometer, by which the tilt of light can be controlled. The two lenses, L_1 and L_2, are used to appropriately scale this angle of the beam as it falls on the objective, which then illuminates and captures light from various points on the sample, with a micron-scale resolution.

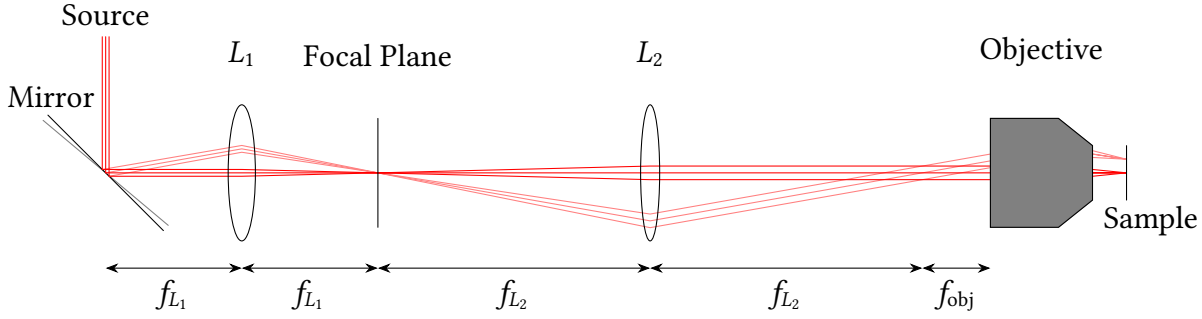

Figure 1.2: Optical Schematic of the Scanning System. Faint lines represent the position of the mirror, and the path of light, when a tilt is applied to the mirror.[25]

In order to study the flakes characterised by this microscope further, a broadband light source is required. This is described in Section 1.4.

1.4 Magnetic and Optical Instrumentation

A variety of opto-mechanical and opto-electronic components were developed as a part of this thesis, such as,

Broadband LED-based Spectroscopic Light Source
There are very few easily available LED light sources that are suitable for spectroscopy, as they either lack stability of light output, or do not cover the visible to near-infrared region fully. This thesis presents the construction of a cost-effective LED light source spanning a spectral range from 400 nm to 1000 nm.

Digital Magnetometers
This thesis also presents the construction of a compact, cost-effective magnetometer.

It is emphasised that apart from the semiconductor devices and some polarising optical elements, all the components were produced by local manufacturers.

1.5 Objectives

This thesis aims to achieve the following objectives:

- to design, construct and test a broadband Sagnac interference based magneto-optic Kerr spectroscope;
- to increase the speed and resolution of an existing scanning photoluminescence imaging microscope; to record photoluminescence images of monolayer regions of transition metal dichalcogenide flakes;
- to design, construct and test a broadband LED light source; and
- to design, construct and test a compact, cost-effective digital magnetometer.

1.6 Scope and Outline

This thesis is divided primarily into four projects, namely; Sagnac Interference-based Magneto-Optic Kerr Spectroscope, Scanning Photoluminescence Imaging Microscope, 2W Broadband LED Light Source for Spectroscopy, and 0.5 T magnetometer.

Chapter 2 presents the techniques used for designing and prototyping the Sagnac interferometry based magneto-optic Kerr spectroscope; the scanning photoluminescence microscope; the broadband LED source and the magnetometer.

Chapter 3 presents the results obtained in carrying out these techniques, whether they were experimental or computational.

Chapter 4 presents the significance of these results, and examines their future prospects.

While the Sagnac interferometer has been assembled, as will be detailed in Subsection 3.1.2, it has not been tested yet, and conclusive results cannot be shown in this thesis. This is due to the current unavailability of a tabletop magnet.

The code controlling the multiple elements of the scanning photoluminescence scanning microscope is listed in Section A.1. The testing procedure of the microscope is described in Subsection 2.2.2, and the results are shown in Subsection 3.2.1. Photoluminescence images taken by the microscope are shown in Subsection 3.2.2. The optical design of the microscope is discussed elsewhere[25], and is beyond the scope of this thesis.

The circuit design, and assembly process of the broadband LED source and magnetometer will be detailed in Section 2.3 and Section 2.4 respectively. The bandwidth, stability, and intensity of the LED source, and its comparison to existing light sources, are shown in Subsection 3.3.2 and Subsection 3.3.3. The calibration of the magnetometer, and its user interface, is described in Subsection 3.4.3 and Subsection 3.4.4, respectively. The firmware for the microcontroller of the magnetometer is described in Section A.3.

Chapter 2

Methods

2.1 Optical Design of the Sagnac Kerr Interferometer

2.1.1 Jones Matrix Analysis

To understand the behaviour of polarised light as it passes through various optical elements, the Jones matrix formalism was used.[12] A beam of polarised light is described by a quantity known as a Jones vector, of the form, $\mathbf{E} = \begin{bmatrix} E_x \\ E_y \end{bmatrix}$, where, E_x and E_y are the complex amplitudes of the electric field vector. Similarly, any optical element through which light passes has a defined matrix $\mathbf{M}$, known as its Jones matrix. $\mathbf{M}$ describes how the polarisation state of the beam is altered, as listed in Table 2.1. When an optical element $(\mathbf{M})$ is illuminated by a beam $(\mathbf{E})$, the emergent beam is described by the product $\mathbf{E}' = \mathbf{M} \times \mathbf{E}$. The measured intensity (I) of a beam is expressed by the norm of its Jones vector,

$$I = \mathbf{E}^* \cdot \mathbf{E} = |E|^2. \tag{2.1}$$

Element	Alignment	Jones Matrix
Polariser	transmission axis $\parallel$ x-axis	$\begin{bmatrix} 1 & 0 \\ 0 & 0 \end{bmatrix}$
Mirrors and beamsplitters at oblique incidence	plane of incidence $\perp$ x-axis ψ and Δ are the ellipsometric parameters	$\begin{bmatrix} \tan\psi e^{i\Delta} & 0 \\ 0 & 1 \end{bmatrix}$
Halfwave Plate	fast axis $\parallel$ x-axis	$\begin{bmatrix} 1 & 0 \\ 0 & -1 \end{bmatrix}$
Quarterwave Plate	fast axis $\parallel$ x-axis	$\begin{bmatrix} 1 & 0 \\ 0 & i \end{bmatrix}$
Magnetised reflective surface	showing Kerr rotation φ and Kerr ellipticity η	$\begin{bmatrix} 1 & -\varphi - i\eta \\ \varphi + i\eta & 1 \end{bmatrix}$

Table 2.1: Jones matrices for various optical elements[12]. It is noted that beamsplitters have different ellipsometry parameters in transmission and reflection. When relevant, this will be denoted by the subscript 'Tr' and 'Rf' respectively.

In order to obtain the Jones matrix of an element that has been rotated by an angle θ along

the optical axis, we can carry out a change of basis from the lab frame $(\left[\begin{smallmatrix}1\\0\end{smallmatrix}\right], \left[\begin{smallmatrix}0\\1\end{smallmatrix}\right])$, to the frame of the element, $\left(\left[\begin{smallmatrix}\cos\theta\\-\sin\theta\end{smallmatrix}\right], \left[\begin{smallmatrix}\sin\theta\\\cos\theta\end{smallmatrix}\right]\right)$, in the following manner. The transformation matrix is defined as

$$\mathbf{R}(\theta) = \begin{bmatrix} \cos\theta & -\sin\theta \\ \sin\theta & \cos\theta \end{bmatrix}, \tag{2.2}$$

and consequently, the Jones matrix $\mathbf{M}'$ of the rotated element is given by the expression,

$$\mathbf{M}' = \mathbf{R}(\theta)^{\mathrm{T}} \mathbf{M}\, \mathbf{R}(\theta).$$

We also used a pair of beam displacers, as will be discussed in Subsection 2.1.2. These are prisms made from single crystals of birefringent materials, such as calcite, or yttrium orthovanadate. They possess the property of splitting a beam into two parallel beams, such that one is polarised in the plane of separation, and one is polarised perpendicular to the plane of separation. The Jones matrix used for this is

$$\mathrm{BD}_{\parallel} = \begin{bmatrix} \cos^2\alpha & \dfrac{\sin\alpha}{2} \\ -\dfrac{\sin\alpha}{2} & \cos^2\alpha \end{bmatrix}, \tag{2.3}$$

$$\mathrm{BD}_{\perp} = \begin{bmatrix} \cos^2(\alpha+90^\circ) & \dfrac{\sin(\alpha+90^\circ)}{2} \\ -\dfrac{\sin(\alpha+90^\circ)}{2} & \sin^2(\alpha+90^\circ) \end{bmatrix}, \tag{2.4}$$

where α is the angle through which the beam displacer has been rotated.

The *Python* library *sympy* for symbolic computation was used to carry out all the matrix multiplication involved in the analysis for our design. The results of this will be discussed in Section 3.1.

2.1.2 Proposed Setup

The configuration of the proposed Sagnac interferometer was determined by Jones matrix analysis, and is shown in Figure 2.1. The matrix analysis for this is presented in Subsection 3.1.1. The light path is described as follows. All angles mentioned are relative to the plane of the setup.

Light from the source is linearly polarised to 0°. This beam is reflected by a beamsplitter, towards a beam displacer. The beam displacer is orientated at 45°, and separates incoming light, into two orthogonally polarised beams, one along 45° (red line) and one along −45° (blue line). The quarterwave plate with its fast axis along 0° converts these two polarisations into left and right circularly polarised light. An achromatic lens, typically an objective lens, focuses them onto the sample, which imparts a relative phase shift to the two beams. Also, due to reflection, the two beams interchange both path and state of polarisation, i.e., the red beam becomes right circular light, and traverses the path that the blue beam took to reach the sample, and vice versa. Upon completing the loop, the two beams are combined at the beam displacer, and transmitted by the beam splitter. By passing them through either a quarterwave plate at 45° or a halfwave plate at 22.5° we can choose to measure either Kerr rotation, φ, or Kerr ellipticity, η, respectively. We use a second beam displacer, right before the spectrometer, in order to separately measure the intensity of the horizontal and vertical polarisation, I_h and I_v respectively. It is from the contrast (δI) of these intensities, as defined below in Eq. 2.5, that

we obtain Kerr rotation or Kerr ellipticity, as will be described in Subsection 3.1.1.

$$\delta I = \frac{I_h - I_v}{I_h + I_v}, \tag{2.5}$$

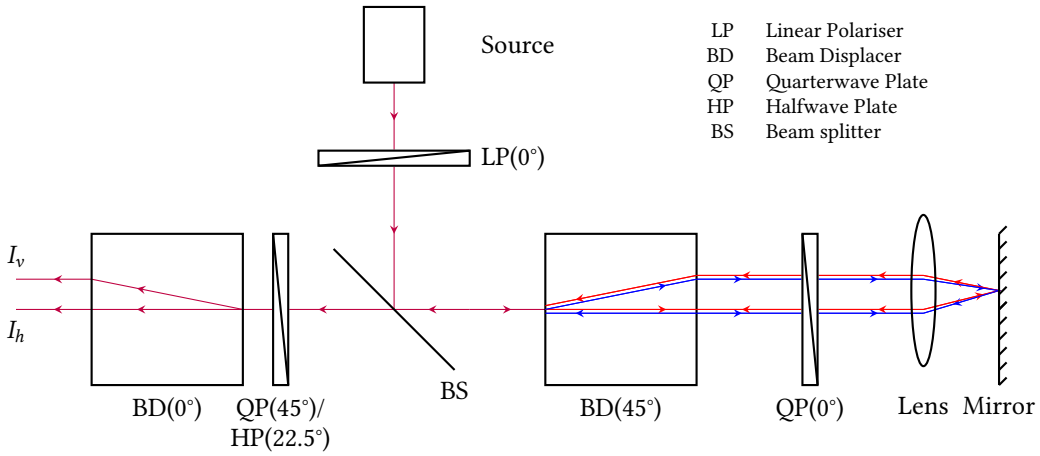

Figure 2.1: Schematic of the Sagnac Kerr interferometer. All angles are relative to the plane of the setup.

2.1.3 Angle Alignment and Measurement Protocol

The reference for the angles of all the polarisation optical elements was the CCD sensor of the spectrometer. Each optical element was aligned, one, by one, in the following manner.

Beam Displacer at 0°

The beam displacer is placed right before the entrance slit of the spectrometer. By doing so, when an unpolarised, monochromatic beam of light, focussed on the entrance slit, is passed through it, two spots corresponding to two orthognal polarisation states are formed on the slit. These spots are viewed on the CCD sensor of the spectrometer, and the beam displacer is rotated until the centre of both these spots lie on the same column of pixels. In this configuration, the displaced beam (known in literature as the extraordinary beam[12]) is polarised parallel to the columns of the CCD. The original beam, known as the ordinary beam, is polarised perpendicular to the columns of the CCD. A representative image of the CCD is shown in Figure 2.2.

Linear Polariser at 0°

The linear polariser is placed before the beam displacer in the optical path, as shown in Figure 2.3b. It is then rotated until the extraordinary ray is extinguished, making its transmission axis lie perpendicular to the CCD columns.

Quarterwave Plate at 0°

The quarterwave plate is placed between the linear polariser and the beam displacer, as shown in Figure 2.3c. It is then rotated until the extraordinary ray is extinguished, making its fast axis lie perpendicular to the CCD columns.

Quarterwave Plate at 45°

Light is passed through the linear polariser, then a beamsplitter, and then through a

quarterwave plate. The light from the quarterwave plate is reflected back through it by a mirror, and reflected by the beamsplitter, through the beam displacer, and then to the spectrometer, as shown in Figure 2.3d. It is then rotated until the extraordinary ray is extinguished, making its fast axis lie at 45° to the columns of the CCD.

Halfwave Plate at 22.5°

The halfwave plate is mounted in a precision rotation mount, and placed between the linear polariser and the beam displacer, as shown in Figure 2.3c. It is then rotated until the extraordinary ray is extinguished, making its fast axis lie perpendicular to the CCD columns.

Then, using the precision rotation mount, it is rotated to 22.5° to the CCD columns.

Beam Displacer at 45°, and Lens

This procedure requires multiple steps. First, a setup as shown in Figure 2.4 is constructed. The lens, placed in a precision *xy*-stage, is focussed onto the mirror. Then, a beam displacer is placed. This produces two beams on the camera, seen as two spots. After placing the quarterwave plate previously aligned to 0° between the beam displacer and the lens, the beam displacer is rotated such that there is only one visible beam on the camera. Finally, the lens is moved along the *xy* stage to return the beam to its initial position, before the placement of the beam displacer. These two elements must be aligned together as the pole of the lens must lie between the two beams produced by the beam displacer.

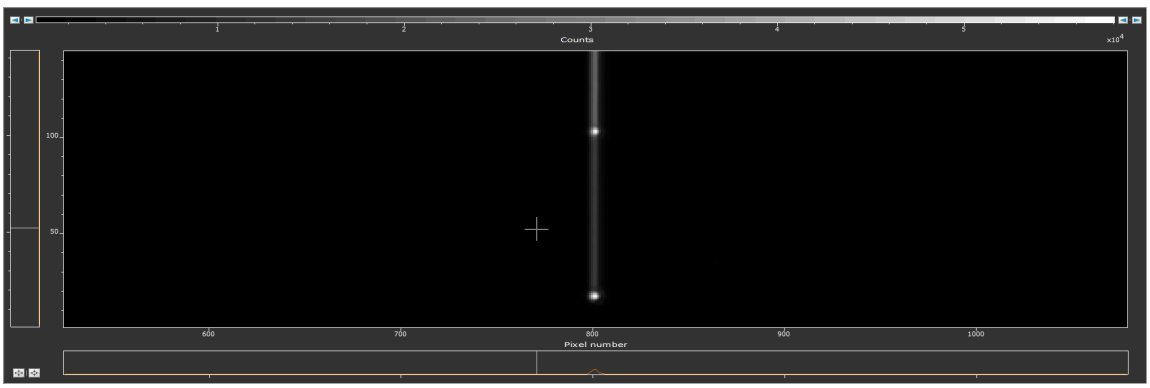

Figure 2.2: Image of Two Spots Formed by Beam Displacer on the CCD of the Spectrometer.

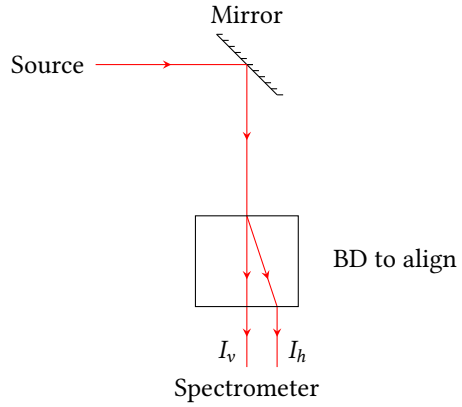

(a) Alignment of beam displacer at 0°

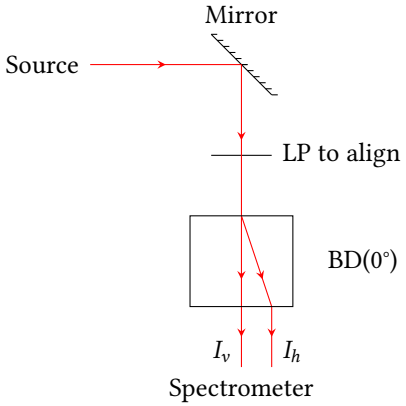

(b) Alignment of linear polariser at 0°

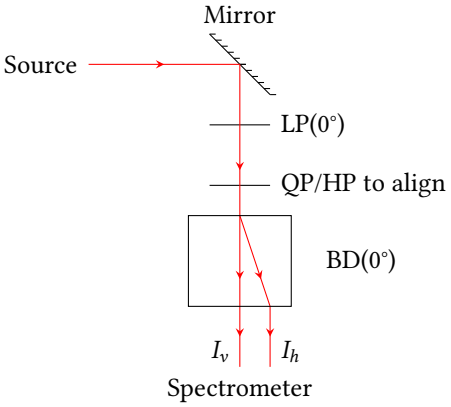

(c) Alignment of Quarterwave/Halfwave Plate at 0°

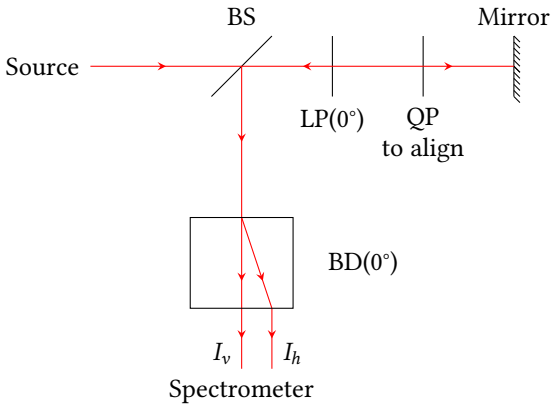

(d) Alignment of Quarterwave Plate at 45°

Figure 2.3: Setups to Align Optical Elements in the Sagnac Kerr Interferometer.

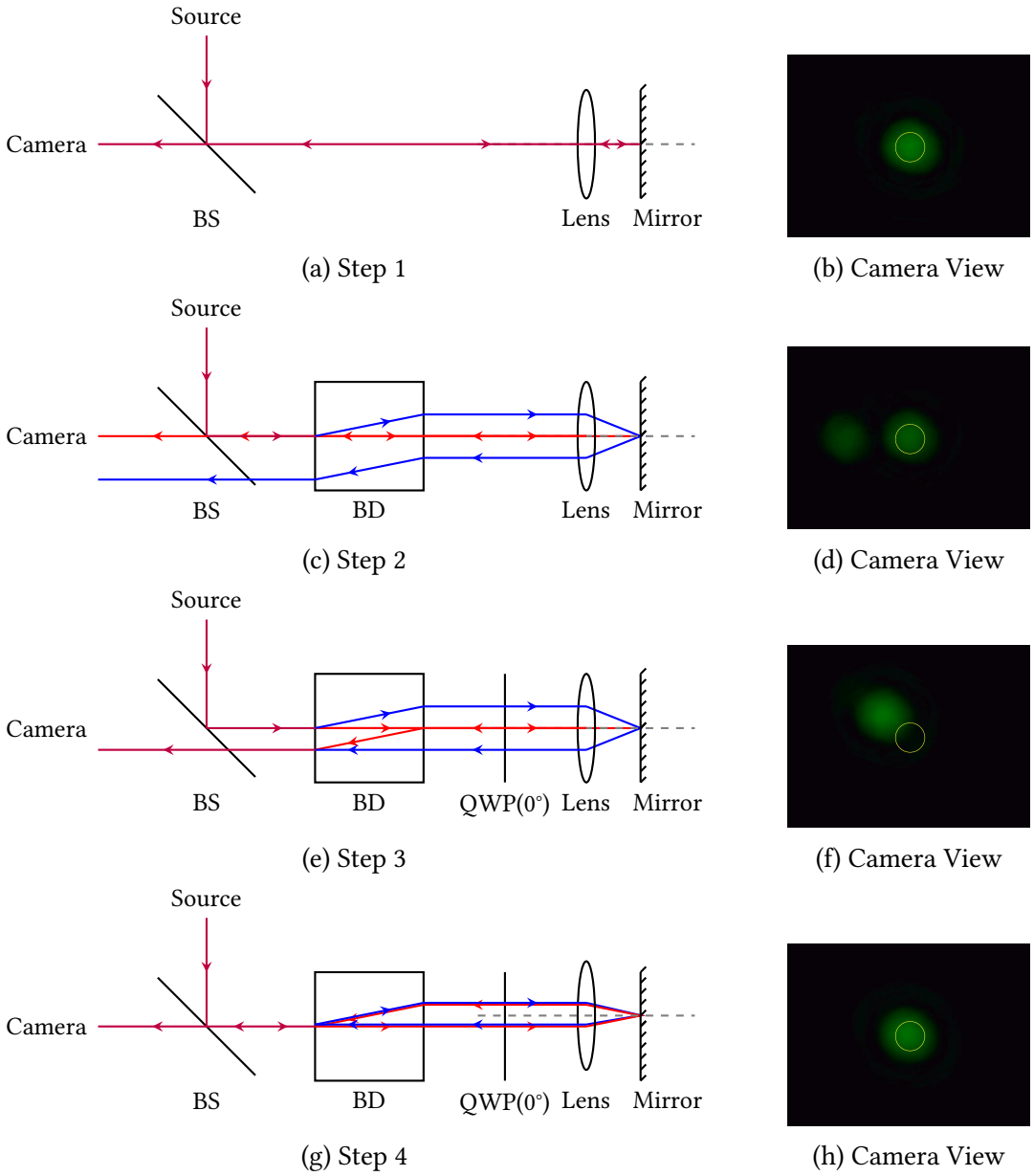

Figure 2.4: Setups to align the beamsplitter to 45°, and the lens to the beamsplitter.

Further measurements could not be conducted without a tabletop electromagnet, which is unavailable at the moment. In the interim, work was done to improve an existing scanning photoluminescence setup, in order to start characterising samples for magneto-optic Kerr measurements. This is described further.

2.2 Scanning Photoluminescence Microscope

2.2.1 Interfacing with Galvanometer Mirrors and Avalanche Photodiode

As described in Section 1.3, the galvo mirrors control the angle of the beam, and correspondingly, the spot on the sample from which the photoluminescence is detected. This detection is done at the avalanche photodiode (APD), after passing the light through a long-pass filter, in order to clean the laser line. It is crucial to ensure that the current through the APD is

read out when the mirrors are stationary, and in their desired position. This requires careful control of the mirrors, and synchronisation with the APD.

An earlier version of this setup, in our lab, was driven with a digital signal generator to control the galvo mirrors, and an Arduino UNO was used for readout from the avalanche photodiode (APD) [in prep]. This setup faced two primary drawbacks. First, the Arduino and the signal generator had to be synchronised in order to accurately match the APD readings with the spot on the sample chosen by the mirrors. Second, the speed of a scan was limited by the Arduino's sampling rate, which is around 10 kHz. This limited the duration of a 1000×1000 pixel scan to a minimum of 30min.

The galvo mirrors used for beam steering are driven by a circuit provided by the manufacturer (GVS002, ThorLabs). In the current work, these are controlled by applying an analog voltage from a data acquisition card (PCIe 6321, National Instruments). The APD (APD410A2, ThorLabs) is integrated into a circuit that converts the current into a voltage, with variable gain, and performs temperature compensation.[26] This is also read out with the NI data acquisition card. While carrying out both these tasks synchronously, a sampling rate of 250 kHz is achieved.[27] This brings the duration of a 1000×1000 pixel scan down to 4 s. Moreover, since the same device is controlling the mirrors and sensing from the APD, both processes can operate from the same clock signal, and are guaranteed to be in sync. NI provides a `Python` package that was used to synchronise and control the application of voltage to the mirrors with the readout from the APD.[28]

In order to calibrate the microscope, a reflectance scan of a micrometer was taken. The known distance between adjacent divisions was compared against the voltages given to the mirrors at those pixel locations. From that, a calibration was carried out, as will be shown in Subsection 3.2.1.

The code underlying the synchronisation and precise control of the galvo mirrors and the APD described in Section A.1. All of the opto-mechanical and opto-electronic components used in the assembly are listed in Table 2.2. Their important specifications are given in Table 2.3.

Component	Manufacturer	Part No
Galvanometer Mounted Mirrors and Driver circuits	ThorLabs	GVS002
Avalanche Photodiode and Amplifier Module	ThorLabs	APD410A2
Data Acquisition Card	National Instruments	PCIe 6321

Table 2.2: List of Components in the Scanning Photoluminescence Microscope.

Component	Specification	Value	Unit
Galvanometer Mounted Mirrors and Driver circuits[29]	Angular Resolution	± 0.0008	°
	Maximum Scan Angle	±12.5	°
Avalanche Photodiode Module[26]	Max Gain	12.5	$kV\,W^{-1}$
	Bandwidth	0 to 10	MHz
Data Acquisition Card[27]	Range	±10	V
	Input Resolution	16	bit
	Input Accuracy	±2.2	mV
	Input Sampling Rate	250	kHz
	Output Resolution	16	bit
	Output Accuracy	±0.3	mV
	Output Sampling Rate	840	kHz

Table 2.3: Important Specifications of the Components used in the Scanning Photoluminescence Microscope

2.2.2 Calibration of the Microscope

In order to measure the distance travelled by the light spot, on the sample, a scan of a stage micrometer was taken. This micrometer has markings at intervals of 10 µm. From the scan settings, the angle between two adjacent pixels were known, and the pixels between adjacent markings were counted. The distance per degree movement is then given as

$$\text{Distance per Degree} = \frac{\text{Distance between Markings}}{\text{Pixels between Markings} \times \text{Angle between Pixels}} \tag{2.6}$$

Theoretically, the distance between two pixels can be expressed as[25]

$$d = 2\frac{f_{L_1} f_{\text{obj}}}{f_{L_2}} \tan\theta, \tag{2.7}$$

where $f_{L_1} = 75\,\text{mm}$ and $f_{L_2} = 200\,\text{mm}$ are the focal lengths of the lenses used in the telescope, as shown in Figure 1.2, $f_{\text{obj}} \sim 7\,\text{mm}$ is the focal length of the objective used, and θ is the rotation of the mirror, per pixel. This evaluates to $\sim$100 µm/°.

In order to take samples characterised by scanning photoluminescence microscopy, and carry out spectroscopic Kerr measurements, a broadband light source is necessary.

2.3 Broadband LED Source

There are no commercially available LED sources that can be used in the entire visible-to-near-infrared range. A single diode, phosphor-coated LED chip manufactured by Epigap, is reported to have the bandwidth required for the spectroscopy of most two-dimensional semiconductors, i.e., 400 nm to 1000 nm.[30] However, this is not packaged with any driver circuitry, and so, a basic tunable constant current power supply was designed and tested.

2.3.1 Circuit Simulation

An op-amp controlled bipolar junction transistor was used as a tunable constant-current power supply[31], in order to control the brightness of the LED. The circuit was simulated using *PSPICE*, in order to determine the parameters of the various passive components. For the active components, *SPICE* models from the manufacturer were used. The model for the diode was unavailable, therefore a *SPICE* diode model was used, the details of which are listed in Table A.1. The results of the simulation are shown in Subsection 3.3.1.

2.3.2 Circuit Testing

After circuit simulation, this was then tested on a breadboard. The current fluctuations and temperature rise over a long period of time was measured using a Keithley 2450 SourceMeter[32], and a TMP6131[33] thermistor onboard the LED module. This was done at various power levels, to ensure that the light output of the source remains stable. The connections for both the current and the temperature measurements are shown in Figure 2.5.

In order to confirm that the onboard thermistor is reading the temperature correctly, a calibrated temperature sensor from a hand-held multimeter was also attached to the LED module, and an independent reading was taken, and verified against the thermistor reading. The results of these tests will be discussed in Section 3.3

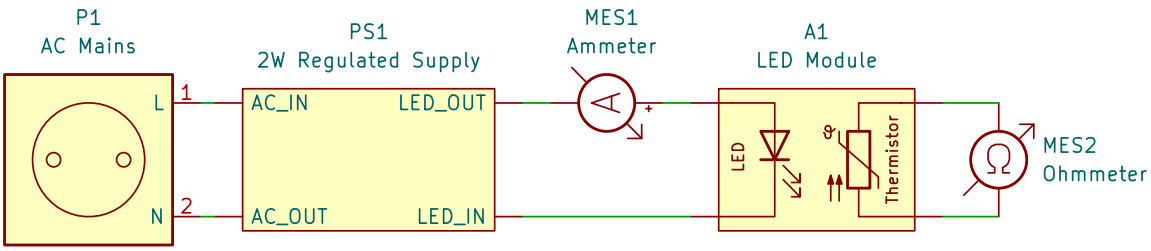

Figure 2.5: Power Supply Testing Schematic: The designed power supply, PS1, converts AC mains voltage into a steady current. This current drives the LED and is measured by ammeter MES1. The resistance of the on-board thermistor is measured by ohmmeter MES2.

Upon satisfactory verification of the circuit, a printed circuit board (PCB) was designed for the power supply circuit, using *KiCAD*. Also, a PCB to hold the LED and thermistor was designed. These were fabricated by local vendors.

2.3.3 Spectral Stability and Intensity

In order to ascertain the utility of the LED module in spectroscopy set-ups, the raw output spectrum was recorded with a homebuilt absorption/transmission/reflection spectroscope. This spectroscope houses a commercial 3 W LED source, as well as a 75 W tungsten filament bulb. The sample-holder was removed, and the emission spectra of both the previous light sources, as well as the constructed light source, were recorded. The intensity of the three sources was compared, as will be described in Subsection 3.3.3.

Further, the spectrum of the constructed LED was recorded at random intervals over a duration of 5 hours in order to measure the fluctuation in the intensity of the constructed LED. This will also be shown in Subsection 3.3.3.

2.3.4 Final Assembly

In order to solder surface mounted components, onto the printed circuit, solder paste was first laid out by a stencil. Each of the components was placed by hand, and the PCB was placed on a hot plate, with a temperature readout. The hotplate was heated up to ≈150 °C for 60 s, and then heated to 180 °C where the solder would start to flow. It was kept at this temperature for 10 s, and then removed from the hot plate and allowed to air cool. This is the reflow process, as suggested by the manufacturers.[30, 33] The through-hole components were soldered by hand.

A custom holder was designed for the LED module, that integrates a heatsink. This is also compatible with the widely used 30 mm cage system. The drawing is shown in Figure 2.6. A custom box was also designed for the power supply circuit.

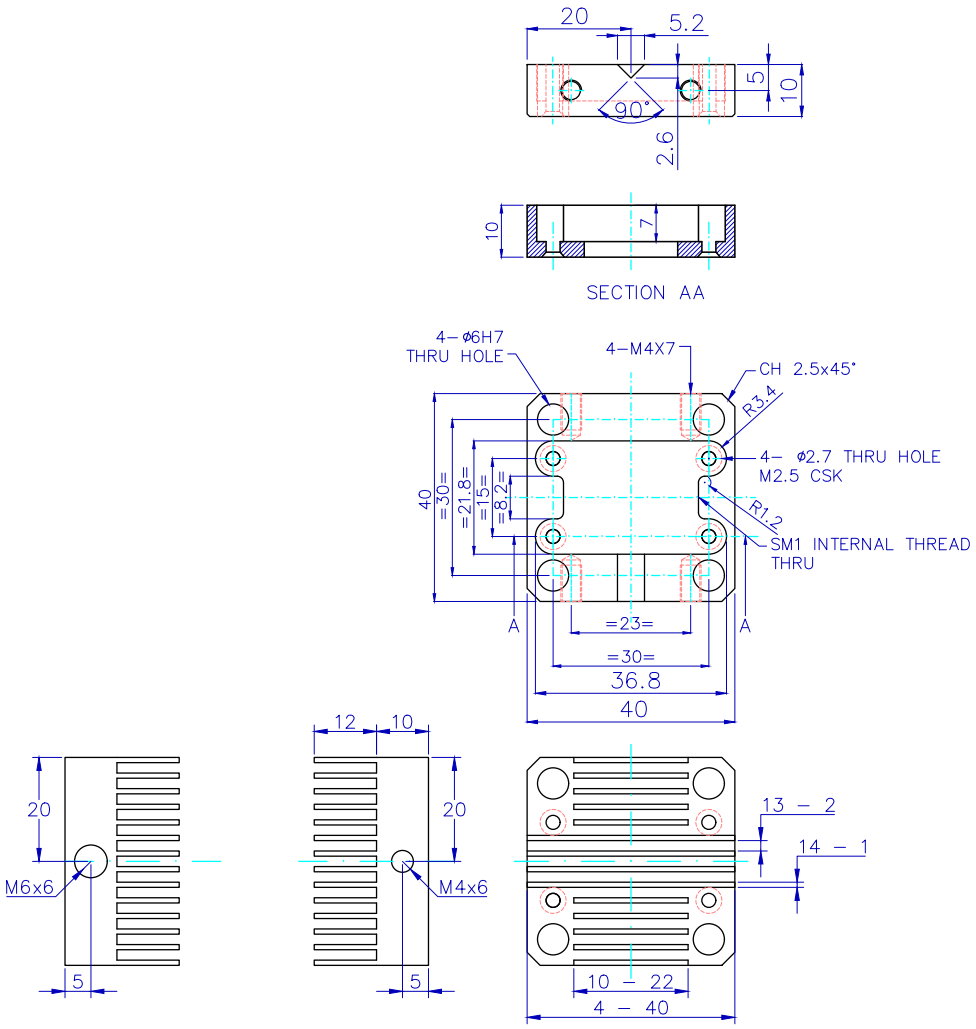

Figure 2.6: Technical Drawing of the LED Module Holder.

2.4 Magnetometer

The circuit design and assembly was done with the same techniques mentioned in Section 2.3. An Allegro A1308 hall sensor[34] is used to convert the magnetic field sensed into a voltage. This is read by a Raspberry Pi Pico microcontroller[**raspberrypi**] module, which has an onboard 12 bit ADC. The firmware for the Pico was written in `MicroPython`.[35] This is

shown in Section A.3. It provides a SCPI interface, the command tree of which is presented in Subsection 3.4.4. The Python library provided in Ref [36] was used to implement the same.

2.4.1 Calibration

To calibrate the sensor, it was placed in the centre of a 1 T electromagnet. The electromagnet and its power supply had been calibrated recently. Using this calibration curve, a sweep of the electromagnet was done, and the readout from the hall sensor was compared. The calibration curve so obtained was stored in the onboard memory of the microcontroller board, for future reference, and is presented in Subsection 3.4.3.

Chapter 3

Results

3.1 Sagnac Kerr Interferometer

3.1.1 Result of Jones Matrix Analysis

In order to evaluate the intensities, I_h and I_v, as shown in Figure 2.1, we must first derive the following expressions.

The light falling on the entrance of the first beam displacer, rotated at 45°, is given as

$$\mathbf{P}_{\text{before loop}} = [\text{BS}_{\text{rf}}][\text{LP}(0^\circ)][\text{Inc}] \tag{3.1}$$

Here, [Inc] is the Jones vector of the light from the source. This is divided by the beam displacer into two beams, one that travels clockwise (cw), and one counter clockwise (ccw). The result of these two paths are given as

$$\mathbf{P}_{\text{cw}} = [\text{BD}_{\perp}(45^\circ)][\text{QP}(0^\circ)][\text{S}][\text{QP}(0^\circ)][\text{BD}_{\parallel}(45^\circ)]\mathbf{P}_{\text{before loop}} \tag{3.2}$$

$$\mathbf{P}_{\text{ccw}} = [\text{BD}_{\parallel}(45^\circ)][\text{QP}(0^\circ)][\text{S}][\text{QP}(0^\circ)][\text{BD}_{\perp}(45^\circ)]\mathbf{P}_{\text{before loop}} \tag{3.3}$$

Upon recombination at the beam displacer, these two Jones vectors can be added. This recombined beam is transmitted by a beam splitter. After it has passed through the quarterwave plate, or the halfwave plate, we can obtain the Jones vectors for $\mathbf{E}_h$ and $\mathbf{E}_v$. $\mathbf{E}_h$ and $\mathbf{E}_v$ are the ordinary and extraordinary beam from the second beam displacer, respectively. Their expressions are given as

$$\mathbf{E}_h^{\text{QP}} = [\text{BD}_{\perp}(0^\circ)][\text{QP}(45^\circ)][\text{BS}_{\text{tr}}]\,(\mathbf{P}_{\text{cw}} + \mathbf{P}_{\text{ccw}}) \tag{3.4}$$

$$\mathbf{E}_v^{\text{QP}} = [\text{BD}_{\parallel}(0^\circ)][\text{QP}(45^\circ)][\text{BS}_{\text{tr}}]\,(\mathbf{P}_{\text{cw}} + \mathbf{P}_{\text{ccw}}) \tag{3.5}$$

and

$$\mathbf{E}_h^{\text{HP}} = [\text{BD}_{\perp}(0^\circ)][\text{HP}(22.5^\circ)][\text{BS}_{\text{tr}}]\,(\mathbf{P}_{\text{cw}} + \mathbf{P}_{\text{ccw}}) \tag{3.6}$$

$$\mathbf{E}_v^{\text{HP}} = [\text{BD}_{\parallel}(0^\circ)][\text{HP}(22.5^\circ)][\text{BS}_{\text{tr}}]\,(\mathbf{P}_{\text{cw}} + \mathbf{P}_{\text{ccw}}) \tag{3.7}$$

From here, we can compute the corresponding intensities, I_h^{QP}, I_v^{QP}, I_h^{HP}, and I_v^{HP}, as well as the contrasts, using Eq. 2.1 and Eq. 2.5, as

$$\delta I_{QP} = \frac{\eta \sin\Delta_{\text{tr}} \tan^2\psi_{\text{tr}}}{\eta^2 + \varphi^2 + \tan\psi_{\text{tr}}} + \frac{\varphi \cos\Delta_{\text{tr}} \tan^2\psi_{\text{tr}}}{\eta^2 + \varphi^2 + \tan\psi_{\text{tr}}} \tag{3.8}$$

$$\delta I_{HP} = \frac{\eta \cos\Delta_{\text{tr}} \tan^2\psi_{\text{tr}}}{\eta^2 + \varphi^2 + \tan\psi_{\text{tr}}} + \frac{\varphi \sin\Delta_{\text{tr}} \tan^2\psi_{\text{tr}}}{\eta^2 + \varphi^2 + \tan\psi_{\text{tr}}} \tag{3.9}$$

Upon neglecting the higher-order terms in φ and η, as they are very small quantities, we obtain the simplified equations,

$$\delta I_{QP} = \eta \sin \Delta_{\text{tr}} \tan \psi_{\text{tr}} + \varphi \cos \Delta_{\text{tr}} \tan \psi_{\text{tr}} \tag{3.10}$$

$$\delta I_{HP} = \eta \cos \Delta_{\text{tr}} \tan \psi_{\text{tr}} + \varphi \sin \Delta_{\text{tr}} \tan \psi_{\text{tr}} \tag{3.11}$$

As we can see, these contrasts only depend on three variables. $\tan \psi_{\text{tr}}$ and $\cos \Delta_{\text{tr}}$ are the ellipsometric parameters of the beamsplitter, in transmission mode. These are can be measured easily for a given beamsplitter. Furthermore, a beamsplitter can be chosen such that it has a very small Δ_{tr}, in which case, the $\sin \Delta_{\text{tr}}$ terms can also be neglected, giving us the equations.

$$\delta I_{QP} = \varphi \cos \Delta_{\text{tr}} \tan \psi_{\text{tr}} \tag{3.12}$$

$$\delta I_{HP} = \eta \cos \Delta_{\text{tr}} \tan \psi_{\text{tr}} \tag{3.13}$$

There is a linear dependence of δI_{QP} on φ, and of δI_{HP} on η.

In order to make a measurement of both Kerr rotation and ellipticity spectra, the following procedure ought to be followed.

First, with the quarterwave plate oriented at 45°, placed after the beamsplitter, the background rotation spectrum of the substrate, such as silicon or sapphire is recorded. Then, the rotation spectrum of the sample is recorded. The quarterwave plate is switched out for the halfwave plate at 22.5°, and the ellipticity spectrum is recorded. Finally, the background ellipticity spectrum is recorded from the substrate. The background spectra are subtracted from their respective signal spectra, in order to obtain the actual Kerr rotation and ellipticity as a function of wavelength.

3.1.2 Assembly of the Sagnac Kerr Interferometer

A prototype of the setup was constructed as shown in Figure 3.1.

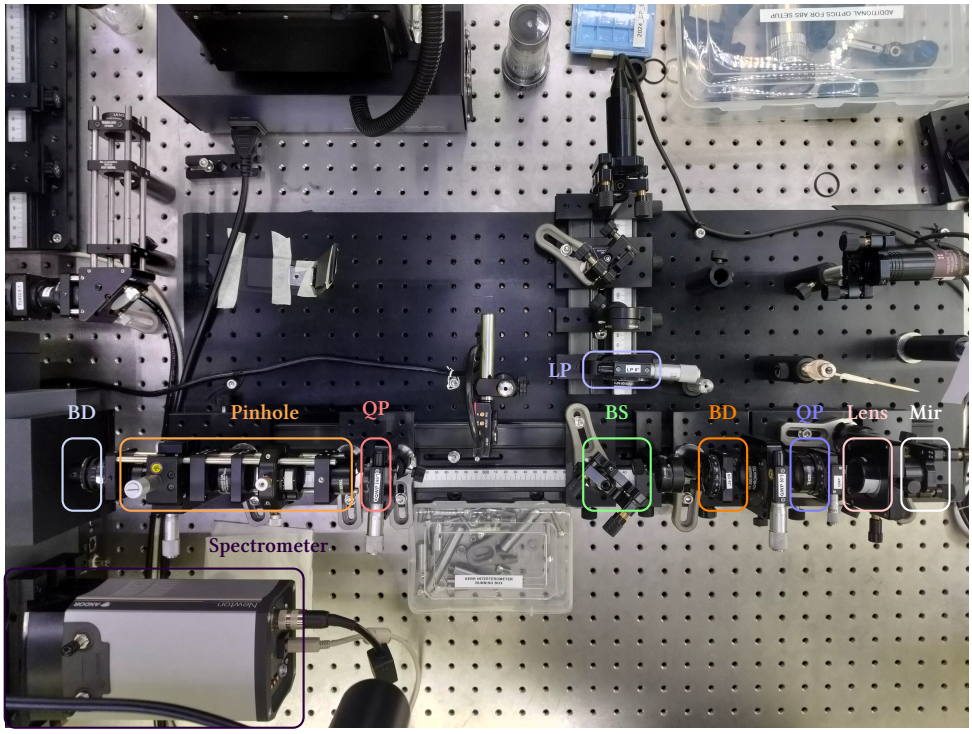

Figure 3.1: Prototype of the Sagnac Kerr Interferometer for Testing.

The testing of this requires a tabletop electromagnet, which was not accessible at the moment. However, the testing technique is as follows. At the mirror, a silicon/silicon dioxide wafer, coated with a few hundred nm of nickel (Ni) will be placed. This will also lie at the centre of the magnet. Kerr rotation spectra, and Kerr ellipticity spectra, as described in Subsection 3.1.1 will be recorded. This will be measured at various fields, and compared against the reported values of Kerr rotation and ellipticity for Ni. Once the interferometer is calibrated, measurements will be carried out on monolayer TMDCs.

In the interim, a scanning photoluminescence microscope was worked on, whose results are shown next.

3.2 Scanning Photoluminescence Microscope

3.2.1 Calibration of the Microscope

The reflectance scan of a stage micrometer, recorded by the scanning photoluminescence microscope, using the controls described in Subsection 2.2.1, is shown in Figure 3.2.

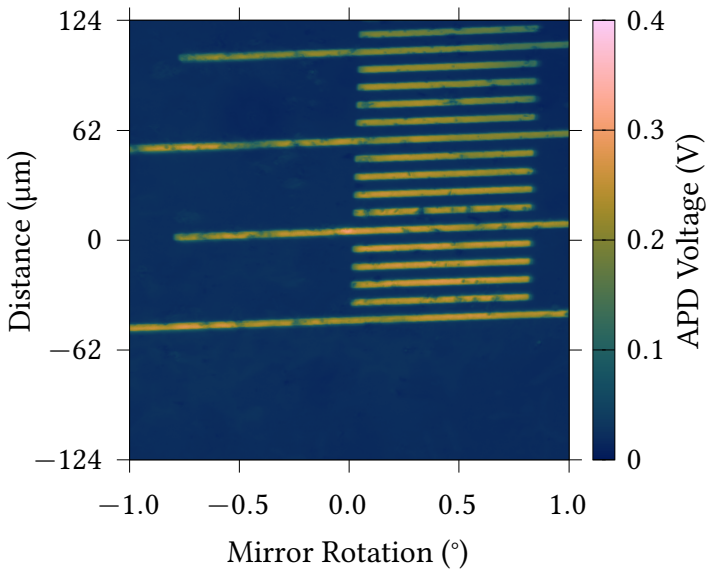

Figure 3.2: Reflectance Scan Image of a Stage Micrometer.

We can see that the image is largely distortion free. Adjacent markings on the micrometer are 10 µm apart. The average number of pixels between two markings is 40.6 µm. The angular resolution of the scan was set at 0.002°. According to Eq. 2.6, this gives us a spatial resolution of 123 µm/°. This is close to the calculated value of 100 µm/°, obtained in Subsection 2.2.2. The difference is primarily due to the error the focal length of the objective, which the manufacturer has not shared. This was then estimated with a scale, and precision greater than 1 mm was not possible.

In order to verify that the APD can sense a photoluminescence signal a scan of a flake of tungsten disulphide was taken.

3.2.2 Photoluminescence Scan of 2D Materials

The exfoliated tungsten disulphide was transferred onto a PDMS gel film. It is known to have a monolayer region, and was expected to emit photoluminescence. The optical image of the flake under white light illumination is shown in Figure 3.3.

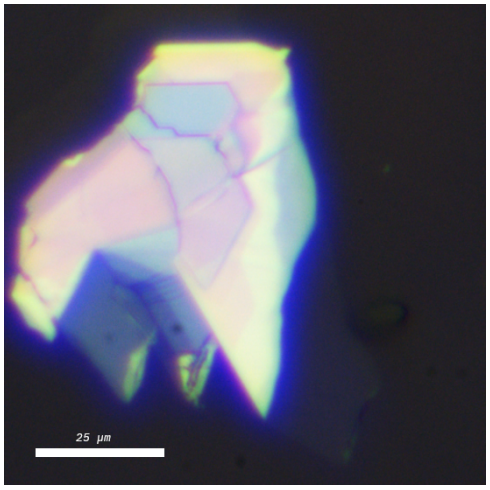

Figure 3.3: Optical Image of a WS_2 Flake on PDMS.

The photoluminescence scan is shown in Figure 3.4. A 532 nm laser was used to excite the sample, and a 550 nm low pass filter was used to remove the laser line. A hotspot in the photoluminescence scan is visible, and is indicative of a monolayer region on the flake. To verify that the photoluminescence was from the monolayer region, a reflectance scan was taken, by removing the low-pass filter, and measuring the intensity of reflected light at each point. This is shown in Figure 3.5.

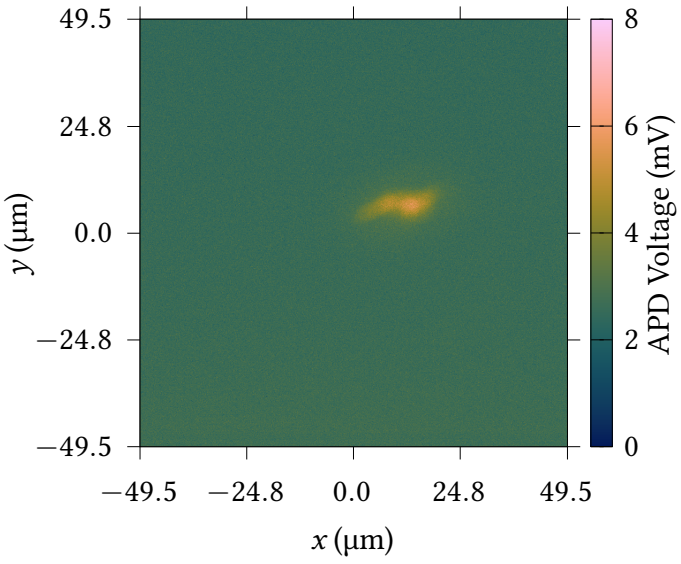

Figure 3.4: Photoluminescence Scan of WS_2 on PDMS. The yellow spot indicates a monolayer.

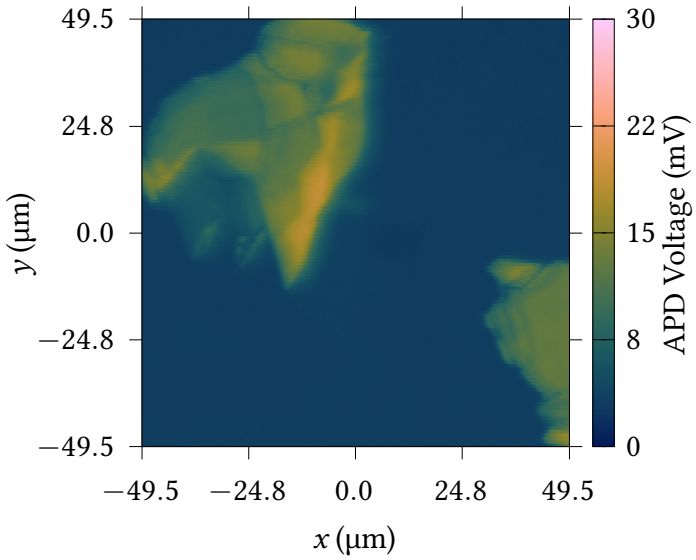

Figure 3.5: Reflectance Scan of WS_2 on PDMS.

This demonstrates that our setup is capable of rapidly identifying monolayer regions in TMDC flakes.

3.3 Broadband LED Power Supply Testing

3.3.1 SPICE Simulations

The circuit used for simulation and further PCB fabrication is shown in Figure 3.6. Its working is explained as follows.

The 1 Ω resistor R5 acts as a current sensing resistor. The voltage across this resistor, i.e. the voltage between the node labeled `I_Sense`, and ground, is directly proportional to the current through it. This is also the current flowing through the LED. The operational amplifier compares the voltage at `I_sense`, to the voltage set by the user, at the potentiometer, RV1, and accordingly, drives a power transistor, Q2, in order to achieve the desired brightness level.

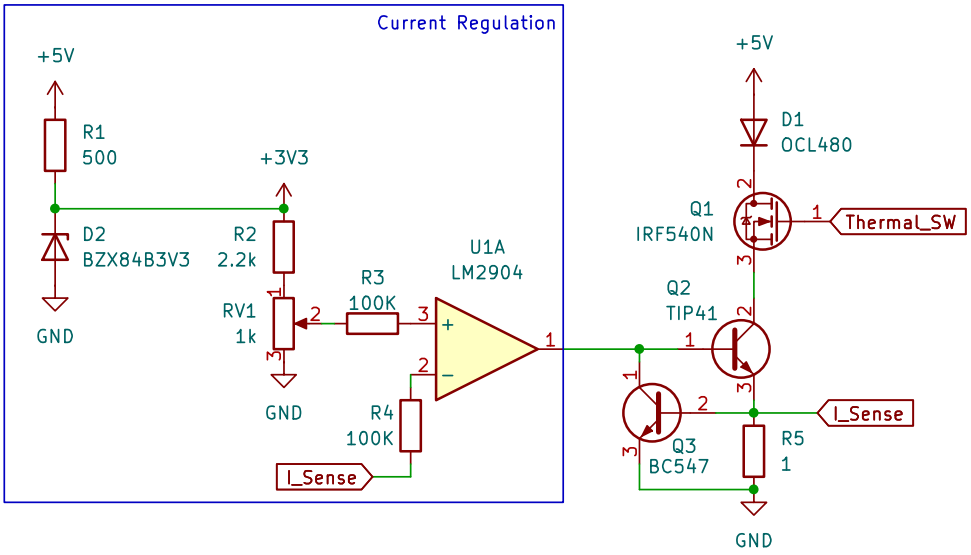

Figure 3.6: Schematic of 2W LED Power Supply

Transistor Q3 is used to prevent excess current from flowing and damaging the diode. It works in the following manner. The device selected is a silicon bipolar junction transistor. These devices start conducting from collector to emitter, once the voltage at the base relative to the emitter is greater than ~0.65 V. By placing R5 across the base and the resistor, we can set a current limit $I_{\max}$ by choosing a value for R5 such that at $I_{\max}$, the voltage across the base and emitter is greater than or equal to 0.65 V. At that point, Q3 starts conducting current away from the base of Q2, such that the current through Q2 can no longer increase.

$$I_{\max} = \frac{R}{0.65\,\mathrm{V}} \tag{3.14}$$

In order to test how well this circuit could control current, a set of *SPICE* simulations were run, to obtain the operating point of the circuit. This was done for a range of values for the resistance of the potentiometer RV1, ranging from 0 % to 120 % of its rated value. At each value, the current through the LED was calculated and plotted in Figure 3.7. Simulating the potentiometer resistance to 120 % is used to account for two things. First, the fact that the tolerance rating of the potentiometer is ±20 %, and second, to ensure that the current-limiting mechanism described above can cap the LED current to the rated maximum of 0.65 A.

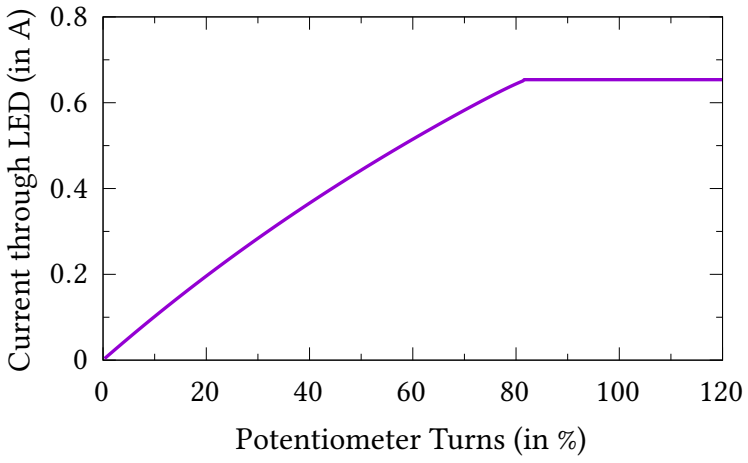

Figure 3.7: Current Through LED as a Function of Potentiometer Resistance.

As we can see, the LED current follows a linear relationship with the turn of the potentiometer, up until the rated maximum current. The current limiting mechanism is activated, and works to protect the LED from burning.

For thermal protection of the LED, the topology showed in Figure 3.8 is used. TH1 is a positive temperature coefficient thermistor mounted next to the LED. The two voltage divider pairs; R6, R11; and R7, TH1 have values chosen such that the comparator, TL331, turns the MOSFET (Q1) off, when TH1 is hotter than 65 °C. This keeps the entire circuit open, and protects the LED from overheating.

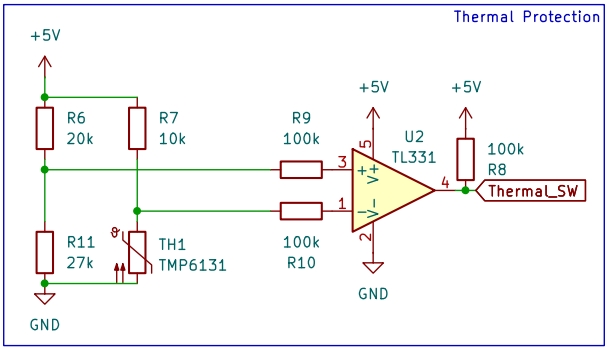

Figure 3.8: Thermal Protection Circuit

3.3.2 Current and Temperature Fluctuations

The current through the LED and the resistance of the onboard thermistor are shown in Figure 3.9.

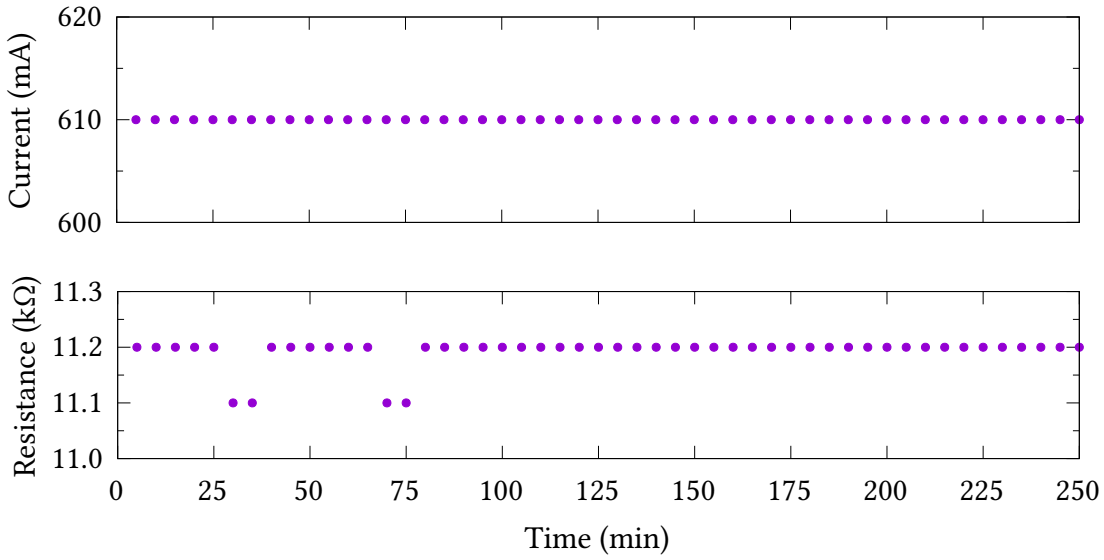

Figure 3.9: Time Series of Current and Thermistor Resistance

.

As we can see, both the current and the resistance were stable to within the precision of the ammeter and ohmmeter used, which were 10 mA and 100 Ω respectively. From the datasheet

of the thermistor[33], the temperature of the LED module can be found to be approximately 40 °C. This is well within the operating temperature of the LED diode, which is 75 °C.[30]

3.3.3 Spectral Stability and Intensity

The comparison of the designed LED source, a commercial 3 W LED source, and a 75 W tungsten filament bulb is shown in Figure 3.10.

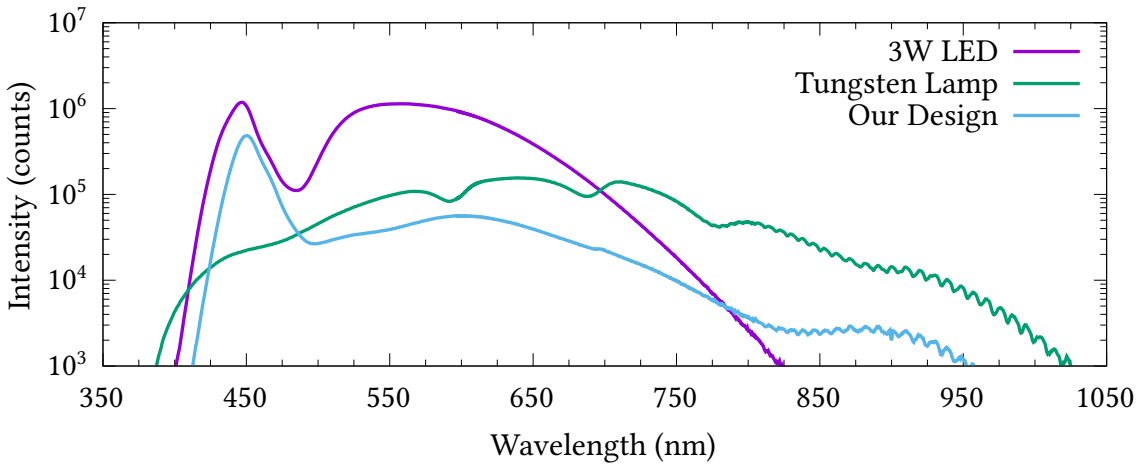

Figure 3.10: Emission Spectra of Various Light Sources used in Spectroscopy.
Acquisition Time: 100 × 0.1 s

.

The spectral width of the designed LED is clearly superior to the commercial 3 W LED, but not as good as the tungsten lamp. However, it is far more efficient than the tungsten lamp, consuming 2 W as opposed to the lamp's 75 W. The designed LED is, however, noticeably darker than both the tungsten lamp and the commercial LED. This can be attributed to the fact that the emitted light diverges strongly, and it is challenging to capture the entire output without using aspheric lenses.

The spectra recorded over 5 hours are plotted, one over another, in Figure 3.11. The spectra effectively lie over one another, showing very little fluctuation.

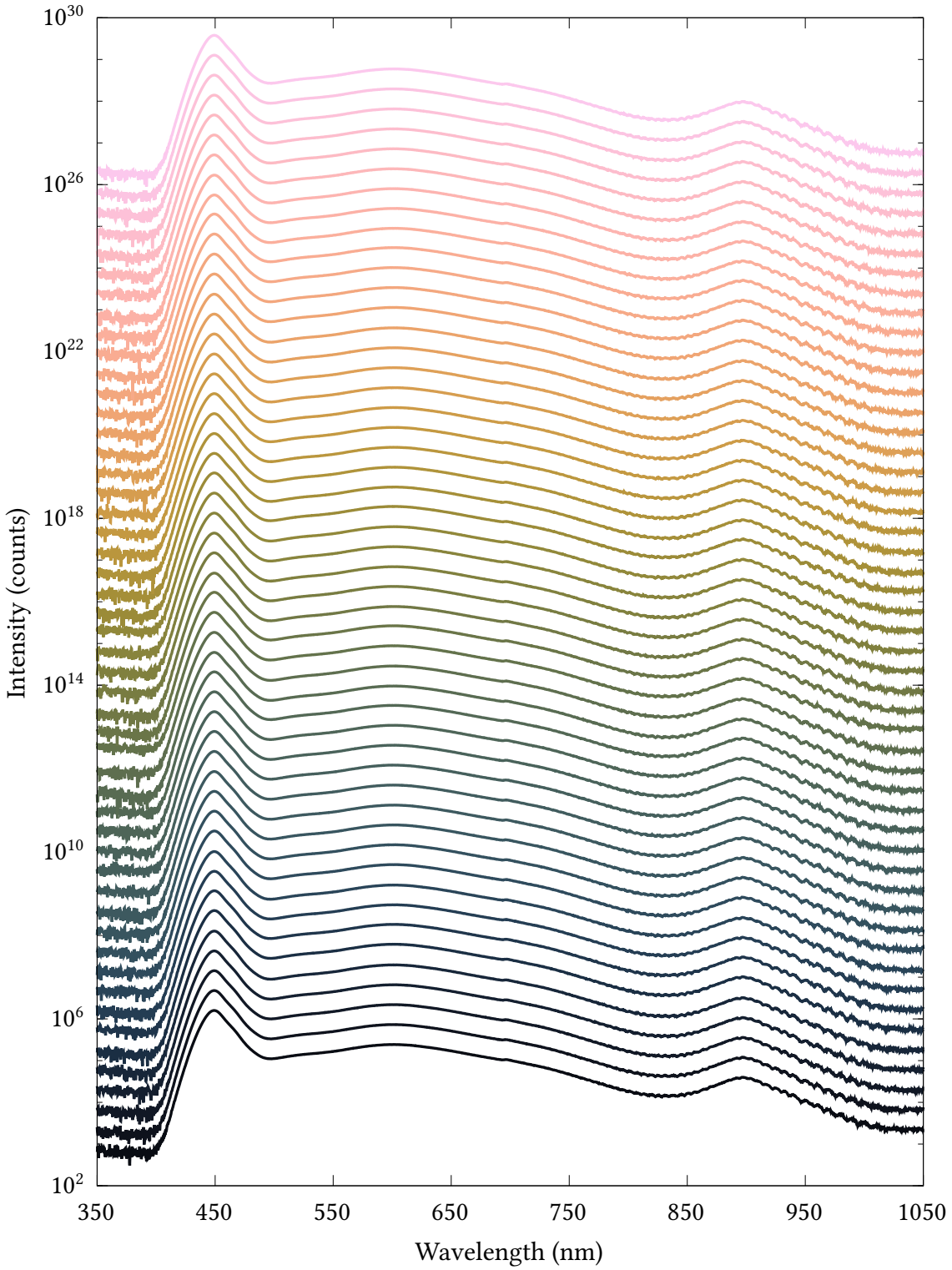

Figure 3.11: Spectra Taken over a 5 Hour Period. Offset for clarity. Adjacent spectra were recorded after a duration of 5 minutes.
Acquisition Time: 100 × 0.1 s

The intensity of the peaks at 450 nm, 600 nm and 900 nm, have been plotted independently in Figure 3.12. We can see clearly that the intensities don't deviate more than 5% from the mean value.

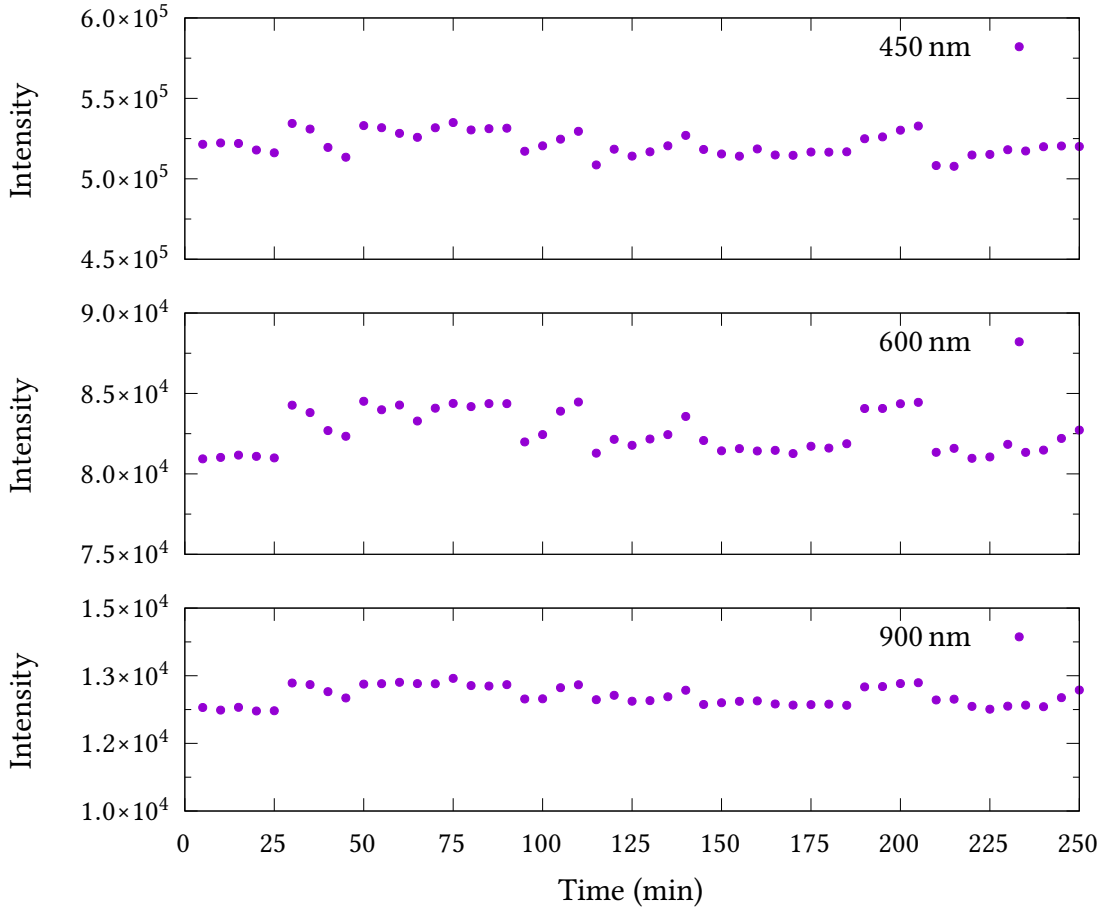

Figure 3.12: Fluctuations of the Intensity of Individual Wavelengths over a 5 hour Period. Acquisition Time: 100 × 0.1 s

3.3.4 Assembled Power Supply and Module

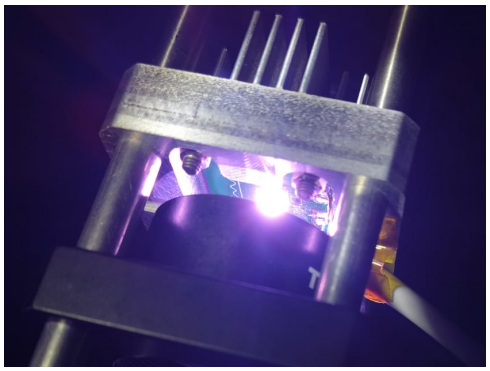

Figure 3.13: The LED Module Integrated into the Cage System

The LED module is shown in Figure 3.14. The PCB is secured to the body of the module through thermally conductive tape, as well as screws. A cover plate has also been designed,

although it has not been manufactured yet.

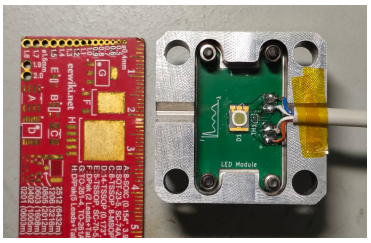

(a) PCB mounted inside.

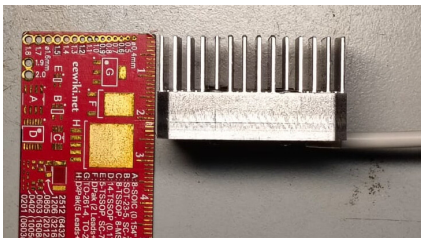

(b) Integrated heatsink.

Figure 3.14: Photographs of Custom-built LED module

The assembled power supply is shown in Figure 3.15. The PCB was prepared as described in Subsection 2.3.4. The user facing side has the port to connect the LED, a knob to control the LED brightness, and an on-off switch.

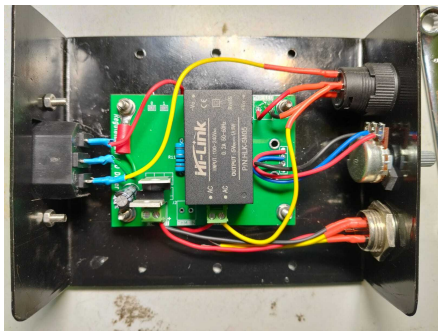

(a) Internal wiring between PCB, potentiometer and sockets.

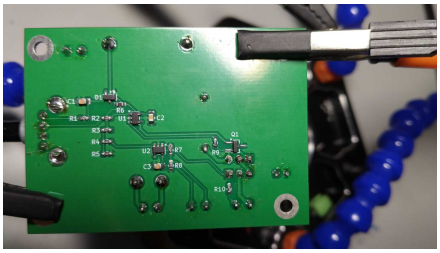

(b) Bottom side of the PCB.

(c) Front of the Case.

(d) Back of the case.

Figure 3.15: Photographs of Assembled LED Power Supply Case.

3.4 Magnetometer

3.4.1 Circuit Design

The schematic of the magnetometer circuit is shown in Figure 3.16, and described below.

The microcontroller board runs with a 3.3 Vdc power supply. However, the hall sensor requires 5 Vdc of power. Hence, a dc-dc boost converter, TPS61322, is used to bring the 3.3 Vdc to 5 Vdc.

A simple voltage-divider circuit consisting of resistors, R1, R2, and R5, is used to convert the voltage from the hall sensor, which ranges from 0.5 V to 4.5 V, to the range of the analog-to-digital converter (ADC), which is 0 V to 3.3 V. A low pass filter, consisting of resistor R4 and capacitor C1, removes any high-frequency noise, and stabilises the voltage at the ADC. The onboard ADC of the Pico has 12 bit of resolution. Readout returns a raw count from the ADC, from which the magnetic field is calculated using the parameters found in Subsection 3.4.3. To ensure that the ADC don't receive any noise from the switching power supplies of the circuit, their supply is regulated against a Zener diode, BZX843V3, which maintains ±1 % of 3.3 V.

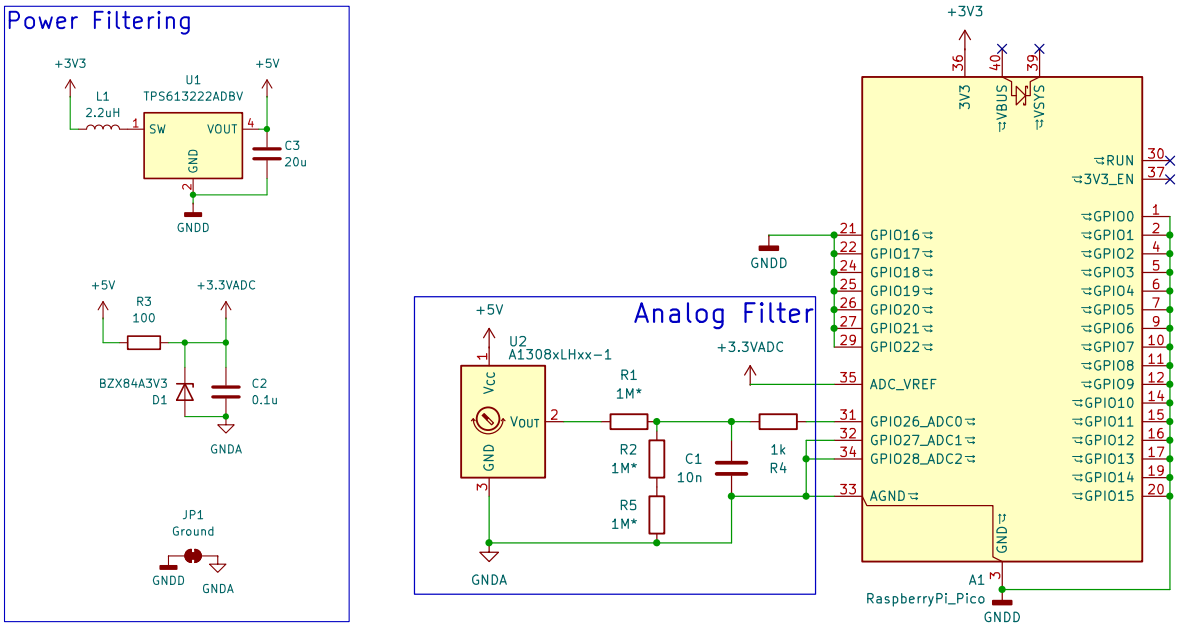

(a) The power filtering sub circuits.

(b) The analog circuit to downconvert the output voltage. Resistors with a star are 0.1 % tolerance.

Figure 3.16: Power and Sensing Circuits for the 0.5 T Magnetometer

3.4.2 Assembly

The assembled magnetometer is shown in Figure 3.17. It is connected to the probe by the screw terminals shown in Figure 3.17a. The analog and power electronics are shown in Figure 3.17b. The analog and power circuits have different ground pours, connected by jumper JP1.

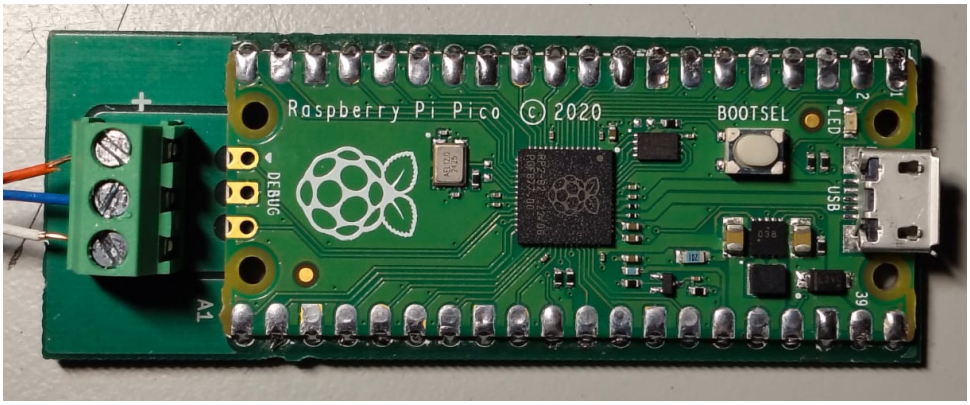

(a) Top Side of the Magnetometer, with the Raspberry Pi Pico Microcontroller Board.

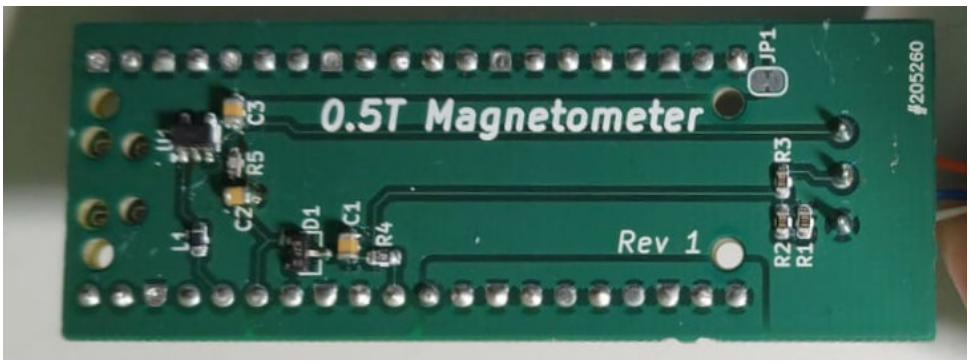

(b) Bottom Side of the Magnetometer.

Figure 3.17: Assembled Magnetometer Circuit

3.4.3 Calibration Curve

The calibration curve measured for the magnetometer is shown in Figure 3.18.

The conversion from ADC counts to magnetic field is by the equation

$$B = m \times C_{\text{ADC}} + c.$$

The inverse equation,

$$C_{\text{ADC}} = m' \times B + c',$$

has been fitted in the graph, and the values m' and c' have been indicated. From these the values, m and c have been obtained to be the following,

$$\begin{aligned} m &= -1.663 \times 10^{-5} \\ c &= 0.534 \end{aligned} \tag{3.15}$$

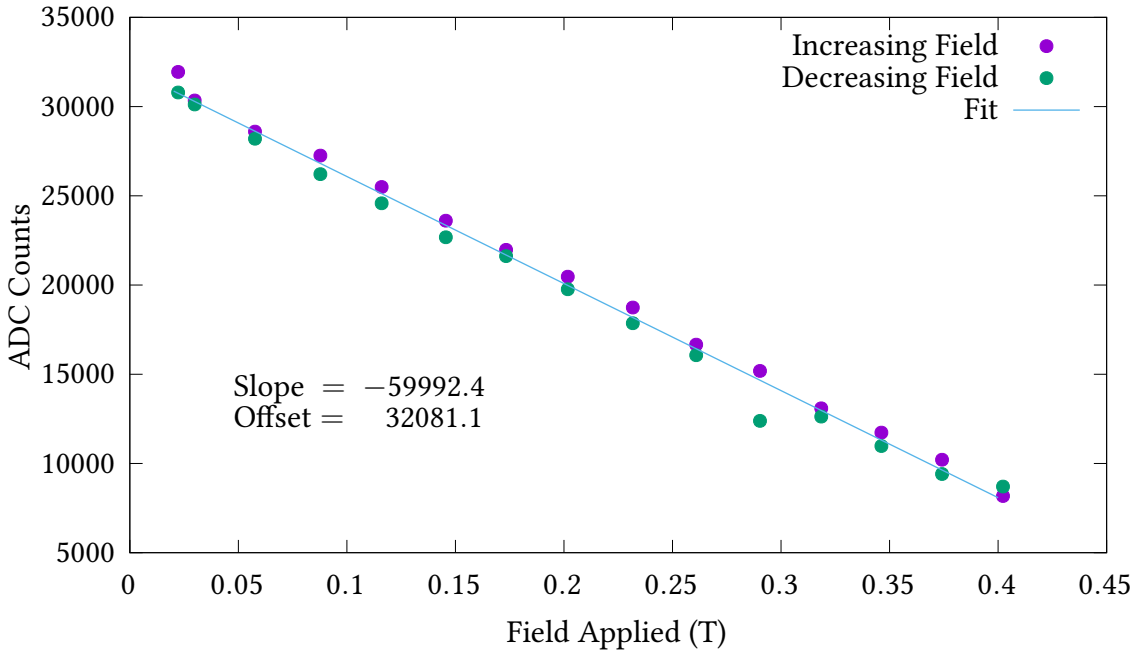

Figure 3.18: Calibration Curve for 0.5 T Magnetometer.

3.4.4 SCPI Interface

Over the standard IEEE 488.1 commands[37], subcommands have been added to the `:MEASure` and `:CONFigure` subsystems. These are described below in Listing 3.1.

Listing 3.1: SCPI Command Tree

```
:MEASure
    :FIELd?             // Measure field.
    :RAW?               // Measure ADC counts.
    :VOLTage?           // Measure voltage.

:CONFigure
    :FIELd          // Configure the ADC to field conversion.
        :OFFSet[?]      // Query or set the conversion offset.
        :SLOPe[?]       // Query or set the conversion factor.
```

Chapter 4

Conclusions

The fulfillment of each objective, as outlined in Section 1.5 is as follows.

Broadband Sagnac Interferometry Based Kerr Spectrometer

The operating principle, and progress on the construction, of a Sagnac interferometry based magneto-optic Kerr effect spectrometer has been demonstrated in Subsection 3.1.1 and Subsection 3.1.2 respectively. This device will be tested using the protocol described in Subsection 3.1.2.

Scanning Photoluminescence Microscope

The high-speed, synchronous control of the galvo mirrors and APD used in the scanning photoluminescence microscope has been demonstrated. The microscope was calibrated, and the pixel to distance ratio was obtained in Subsection 3.2.1. Furthermore, its use in identifying monolayer regions of thin semiconductor flakes is highlighted in Subsection 3.2.2.

The next goal in this project is to incorporate a spectrometer in order to construct hyperspectral photoluminescence images at the micron scale.

Broadband LED Source

A broadband 400 nm to 1000 nm LED source was designed. Its suitability for spectroscopic measurements, i.e., the bandwidth and stability of the emitted spectrum, has been demonstrated in Subsection 3.3.3.

The next goal in this project is to construct an optical assembly that can efficiently collimate the light emitted by this LED in order to enhance its brightness.

Compact Digital Magnetometer

A 0 T to 0.5 T digital magnetometer has been designed and constructed. Its calibration has been demonstrated in Subsection 3.4.3. The case for both the probe and the magnetometer need to be designed.

The design of a 0 T to 3 T magnetometer is under progress.

Bibliography

[1] N. Miura. *Physics of semiconductors in high magnetic fields*. en. Series on semiconductor science and technology 15. Oxford: Oxford university press, 2008. ISBN: 978-0-19-851756-6.

[2] A. K. Zvezdin and V. A. Kotov. *Modern Magnetooptics and Magnetooptical Materials*. Boca Raton: CRC Press, Jan. 1997. ISBN: 978-0-367-80260-8. DOI: 10.1201/9780367802608.

[3] M. Faraday. "I. Experimental researches in electricity.—Nineteenth series". In: *Phil. Trans. R. Soc.* 136 (Dec. 1846), pp. 1–20. DOI: 10.1098/rstl.1846.0001.

[4] J. Kerr. "XLIII. On rotation of the plane of polarization by reflection from the pole of a magnet". In: *The London, Edinburgh, and Dublin Philosophical Magazine and Journal of Science* 3.19 (May 1877), pp. 321–343. DOI: 10.1080/14786447708639245.

[5] B. Carey et al. "Giant Faraday rotation in atomically thin semiconductors". en. In: *Nat Commun* 15.1 (Apr. 2024), p. 3082. DOI: 10.1038/s41467-024-47294-5.

[6] A. Arora et al. "Magneto-optical Kerr effect spectroscopy based study of Landé g-factor for holes in GaAs/AlGaAs single quantum wells under low magnetic fields". In: *J. Appl. Phys.* 113.21 (June 2013), p. 213505. DOI: 10.1063/1.4808302.

[7] A. Kapitulnik, J. S. Dodge, and M. M. Fejer. "High-resolution magneto-optic measurements with a Sagnac interferometer (invited)". en. In: *Journal of Applied Physics* 75.10 (May 1994), pp. 6872–6877. DOI: 10.1063/1.356814.

[8] G. Sagnac. "The luminiferous aether demonstrated by the effect of the wind relative to the aether in a uniformly rotating interferometer". In: *Comptes Rendus* 157 (1913), pp. 708 –710.

[9] A. Fried, M. Fejer, and A. Kapitulnik. "A scanning, all-fiber Sagnac interferometer for high resolution magneto-optic measurements at 820 nm". In: *Review of Scientific Instruments* 85.10 (Oct. 2014), p. 103707. DOI: 10.1063/1.4897184.

[10] J. Xia et al. "Modified Sagnac interferometer for high-sensitivity magneto-optic measurements at cryogenic temperatures". In: *Applied Physics Letters* 89.6 (Aug. 2006), p. 062508. DOI: 10.1063/1.2336620.

[11] ThorLabs. *850 nm 40 GHz LiNbO3 Intensity Modulators*. June 2023.

[12] E. Hecht. *Optics*. en. 5 ed. Boston: Pearson Education, Inc, 2017. ISBN: 978-0-13-397722-6.

[13] B. E. A. Saleh and M. C. Teich. *Fundamentals of Photonics*. 2019.

[14] M. Born, E. Wolf, and A. B. Bhatia. *Principles of optics: electromagnetic theory of propagation, interference, and diffraction of light*. en. Seventh (expanded) anniversary edition, 60th anniversary edition. Cambridge: Cambridge University Press, 2019. ISBN: 978-1-108-76991-4.

[15] K. Sato and T. Ishibashi. "Fundamentals of Magneto-Optical Spectroscopy". en. In: *Front. Phys.* 10 (Oct. 2022), p. 946515. DOI: 10.3389/fphy.2022.946515.

[16] S. Ezekiel, H. J. Arditty, and A. L. Schawlow, eds. *Fiber-Optic Rotation Sensors and Related Technologies: Proceedings of the First International Conference MIT, Cambridge, Mass., USA, November 9–11, 1981.* en. Vol. 32. Springer Series in Optical Sciences. Berlin, Heidelberg: Springer Berlin Heidelberg, 1982. ISBN: 978-3-662-13527-3 978-3-540-39490-7. DOI: 10.1007/978-3-540-39490-7.

[17] S. Spielman et al. "Measurement of the spontaneous polar Kerr effect in YBa2Cu3O7 and Bi2Sr2CaCu2O8". In: *Phys. Rev. Lett.* 68.23 (June 1992), pp. 3472–3475. DOI: 10.1103/PhysRevLett.68.3472.

[18] D. H. Hurley and O. B. Wright. "Detection of ultrafast phenomena by use of a modified Sagnac interferometer". EN. In: *Opt. Lett., OL* 24.18 (Sept. 1999), pp. 1305–1307. DOI: 10.1364/OL.24.001305.

[19] Y. Shin and J.-W. Kim. "Magneto-optical Kerr effect measurement in ultrafast Sagnac interferometry using the Jones matrix approach". en. In: *Opt. Lett.* 46.14 (July 2021), p. 3364. DOI: 10.1364/OL.429988.

[20] M. Molas et al. "Energy Spectrum of Two-Dimensional Excitons in a Nonuniform Dielectric Medium". In: *Phys. Rev. Lett.* 123.13 (Sept. 2019), p. 136801. DOI: 10.1103/PhysRevLett.123.136801.

[21] A. Arora et al. "Dark trions govern the temperature-dependent optical absorption and emission of doped atomically thin semiconductors". en. In: *Phys. Rev. B* 101.24 (June 2020), p. 241413. DOI: 10.1103/PhysRevB.101.241413.

[22] M. Koperski et al. "Orbital, spin and valley contributions to Zeeman splitting of excitonic resonances in MoSe2, WSe2 and WS2 Monolayers". en. In: *2D Mater.* 6.1 (Oct. 2018), p. 015001. DOI: 10.1088/2053-1583/aae14b.

[23] A. Arora. "Magneto-optics of layered two-dimensional semiconductors and heterostructures: Progress and prospects". In: *Journal of Applied Physics* 129.12 (Mar. 2021), p. 120902. DOI: 10.1063/5.0042683.

[24] M. R. Molas et al. "The optical response of monolayer, few-layer and bulk tungsten disulfide". en. In: *Nanoscale* 9.35 (2017), pp. 13128–13141. DOI: 10.1039/C7NR04672C.

[25] R. Schneider. "Aufbau eines Laser Scanning Konfokalmikroskops". Bachelor. Technische Universität Chemnitz, Aug. 2012.

[26] ThorLabs. *Adjustable Gain Avalanche Photodiode.* Feb. 2020.

[27] N. Instruments. *NI PCIe-6321.* Apr. 2025.

[28] *ni/nidaqmx-python.* Mar. 2026.

[29] ThorLabs. *Small Beam Diameter Scanning Galvo Systems.* Aug. 2024.

[30] Epigap. *High Power Broadband LED with Glob Top Visible and Infrared Light Emission.* July 2025.

[31] P. Horowitz and W. Hill. *The art of electronics.* en. Third edition, 19th printing with corrections. New York: Cambridge University Press, 2022. ISBN: 978-0-521-80926-9.

[32] Keithley. *Interactive SourceMeasure Instrument.*

[33] T. Instruments. *Linear Thermistor.* Nov. 2023.

[34] A. Microsystems. *Linear Hall-Effect Sensor ICs with Analog Output Available in a Miniature, Low-Profile Surface-Mount Package*. July 2024.

[35] *micropython/micropython*. Mar. 2026.

[36] *stonerlab/MicroPython_SCPI*. Dec. 2024.

[37] S. Consortium. *Standard Commands for Programmable Instruments*. May 1999.

Appendix A

Code

A.1 Hyperspectral Imaging Setup

```
import argparse
from time import monotonic
from math import floor

import numpy as np
import matplotlib.pyplot as plt
import matplotlib.animation as anim
import nidaqmx as ni
from nidaqmx.constants import (
    AcquisitionType,
    DigitalWidthUnits,
    TerminalConfiguration
    )

def Scan(
  ampl,
  step = 0.2,
  aq_time_ms = 0.1
  dry = False,
  average = 0,
):
  ampl = ampl / 0.8
  step = step / 0.8

  a = np.arange(
      -ampl,
      ampl + step,
      step,
      )
  l = len(a)

  frames = 2 + average

  x, y = np.meshgrid(a, a)

  x, y = (np.repeat(x, 2, axis=0), np.repeat(y, 2, axis=0))

  for i in range(l*2):
    x[i] = x[i] if i % 2 == 0 else np.flip(x[i])
```

```
  if dry:
    fig, axes = plt.subplots(ncols=2)
    axes[0].imshow(x)
    axes[0].set_title("x")
    axes[1].imshow(y)
    axes[1].set_title("y")
    plt.show()

  x, y = (np.repeat(x, frames), np.repeat(y, frames))

  if dry:
    z = x + y
    z = np.reshape(z, (2*l, l, 2))[:, :, 1]
    v = np.array([z[2*i] for i in range(l)])
    plt.imshow(v)
    plt.show()
    return

  samps = len(x)
  rate = 3e3 / aq_time_ms
  scan_duration_ms = samps * aq_time_ms

  z = x + y

  with (
      ni.Task() as ao,
      ni.Task() as ai
      ):

    ao.ao_channels.add_ao_voltage_chan("Dev1/ao0:1")

    ai.ai_channels.add_ai_voltage_chan(
            "Dev1/ai0",
            terminal_config=TerminalConfiguration.DIFF
            )

    ai.ai_channels["Dev1/ai0"].ai_rng_high = 1
    ai.ai_channels["Dev1/ai0"].ai_rng_low = -1

    ao.timing.cfg_samp_clk_timing(
      rate,
      sample_mode = AcquisitionType.FINITE,
      samps_per_chan = samps
      )

    ai.timing.cfg_samp_clk_timing(
      rate,
      sample_mode = AcquisitionType.FINITE,
      samps_per_chan = samps
      )
    ao.triggers.start_trigger.cfg_dig_edge_start_trig(
            ai.triggers.start_trigger.term
            )
    ai.triggers.start_trigger.delay_units = DigitalWidthUnits.SAMPLE_CLOCK_PERIODS
    ai.triggers.start_trigger.delay = 0.5

    ao.write(np.array([x, y]), auto_start=False)
```

```
    ao.start()
    z = ai.read(samps, timeout = scan_duration_ms / 1e3)
    ao.wait_until_done(timeout = scan_duration_ms / 1e3)

    ao.write([[0], [0]])

  if average:
    z = np.reshape(z, (2*l, l, frames))[:, :, 1:]
    z = np.average(z, axis=2)
  else:
    z = np.reshape(z, (2*l, l, frames))[:, :, 1]
  v = np.array([z[2*i] for i in range(l)])
  return v

def AlignAPD(channel='0', frequency=1, amplitude=0.2, step=0.002):
  read_rate_hz = 20
  disp_duration_sec = 6
  p = 1 / frequency

  disp_duration_sec * read_rate_hz
  xlim = disp_duration_sec

  ampl = amplitude / 0.8
  step = step / 0.8

  with (
      ni.Task() as apd,
      ni.Task() as gal,
  ):
    apd.ai_channels.add_ai_voltage_chan(
            "Dev1/ai0",
            terminal_config=TerminalConfiguration.DIFF
            )
    gal.ao_channels.add_ao_voltage_chan(f"Dev1/ao{channel}")

    fig, ax = plt.subplots()
    figManager = plt.get_current_fig_manager()
    figManager.full_screen_toggle()

    val = 0
    add = True
    t_zero = monotonic()

    line, = ax.plot([0], [0])

    ax.set_title("Live APD Readout")

    ax.set_xlim(0, xlim)
    ax.set_ylim(0, 1)

    ax.set_xlabel("Time (in seconds)")
    ax.set_ylabel("APD Output (in volts)")

    def update(frame):
      nonlocal line, gal, apd, val, add, t_zero
      t = monotonic() - t_zero
```

```
      val = ampl * ( abs( 2 * ( t / p - floor( t / p + 1/2 ) ) ) - 1/2 )

      try:
        gal.write(val)
        volt = apd.read()
      except EOFError:
        plt.close()

      x, y = line.get_data()

      x = np.append(x, [t])
      y = np.append(y, [volt])

      x = x[-round(disp_duration_sec*read_rate_hz*1.5):]
      y = y[-round(disp_duration_sec*read_rate_hz*1.5):]

      line.set_data(x, y)

      """
      bot, top = ax.get_ylim()
      if abs(volt) > top:
        ax.set_ylim(bot, volt + 0.1)
      elif abs(volt) > bot:
        ax.set_ylim(volt - 0.1, top)
      """

      left, right = ax.get_xlim()
      if t > right:
        left  += 1
        right += 1

        ax.set_xlim(left, right)

      return (line, )

    anim.FuncAnimation(fig=fig, func=update, interval=10, blit=False)
    plt.show()
    apd.close()
    gal.write(0)
    gal.close()

  return

def CleanUp():
  with ni.Task() as ao:
    ao.ao_channels.add_ao_voltage_chan("Dev1/ao0:1")
    ao.write([0, 0])
    ao.wait_until_done()
  return

if __name__ == "__main__":
  parser = argparse.ArgumentParser()
  parser.add_argument(
                "mode",
                type=str,
                help="Select mode, scanning, dry or APD alignment.")
  parser.add_argument(
                '-a',
```

```
                "--amplitude",
                type=float,
                help="Amplitude of the beam, in degrees.")
parser.add_argument(
                '-t',
                "--time_step",
                type=float,
                help="Acquisition time for each pixel, in milliseconds.")
parser.add_argument(
                '-y',
                "--angl_step",
                type=float,
                help="Angular separation between pixels, in degrees.")
parser.add_argument(
                '-f',
                "--frequency",
                type=float,
                help="Frequency to vibrate mirror, in Hz.")
parser.add_argument(
                '-v',
                "--average",
                type=int,
                default=0,
  help="Choose number of frames to average over.")
parser.add_argument(
                '-c',
                "--channel",
                type=str,
                help="Channel to align to APD.")
parser.add_argument(
                '-o',
                "--output",
                help="Filename to save data.")
parser.add_argument(
                '-s',
                "--show",
                help="Show map when done.", action="store_true")

args = parser.parse_args()

try:
  match (args.mode):
    case ('scan'):
      if not ( args.show or (args.output is None) ):
        output_warning = (
          "The output will not be shown or saved, and will be forgotten, for …ever\n"
          "Don't."
          )
        input(output_warning)

      z = Scan(
        args.amplitude,
        step=args.angl_step,
        aq_time_ms = args.time_step,
        average=args.average)
      CleanUp()

      if args.show:
```

```
          plt.pcolormesh(z)
          plt.colorbar()
          plt.gca().set_aspect('equal')
          plt.show()

        average = args.average + 1

        if args.output:
          np.savetxt(
              args.output,
              z,
              delimiter = ",",
              header = (
                f"Amplitude = {args.amplitude}°,\n"
                f"Acquisition time = {args.time_step}ms\n"
                f"Angular Resolution = {args.angl_step}°\n"
                f"Average = {average}"
              )

      case ('align'):
        AlignAPD(args.channel, args.frequency, args.amplitude)
        CleanUp()

      case ('dry'):
        Scan(args.amplitude, step=args.angl_step, dry=True)

  except Exception as E:
    print(E)
    CleanUp()
```

A.2 Spice Simulations

Parameter	Value
I_REV_LEAK	1E-5
IF_SPEC	0.65
V_BR	600
VJ_KNEE	2.7
VJ_SPEC	3.1

Table A.1: SPICE Parameters for the Diode[30]

A.3 Magnetometer Firmware

```
from time import sleep_ms
sleep_ms(500)

from machine import ADC, Pin
from instr import SCPI, Command, BuildCommands

@BuildCommands
class Magnetometer(SCPI):
  def assign_adc(self, adc_pin):
    try:
      self.adc = ADC(Pin(adc_pin))
    except:
      exit()
    return

  def load_cal(self):
    with open("cal.txt", 'r') as cal_file:
      self.m = float(cal_file.readline())
      self.c = float(cal_file.readline())

  def read(self):
    self.reading = self.adc.read_u16()
    self.volts   = 3.3 * self.reading / 65535
    self.teslas  = self.reading * self.m - self.c
    return

  @Command(command="CONFigure:FIELd:SLOPe?")
  async def get_slope(self):
    print(self.m)
    return

  @Command(command="CONFigure:FIELd:OFFSet?")
  async def get_offset(self):
    print(self.c)
    return

  @Command(command="CONFigure:FIELd:SLOPe")
  async def set_slope(self, m):
    self.m = m
    with open("cal.txt", 'w') as cal_file:
      cal_file.write(self.m)
      cal_file.write(self.c)
    return

  @Command(command="CONFigure:FIELd:OFFSet")
  async def set_offset(self, m):
    self.c = c
    with open("cal.txt", 'w') as cal_file:
      cal_file.write(self.m)
      cal_file.write(self.c)
    return

  @Command(command="MEASure:RAW?")
  async def read_raw(self):
    self.read()
    print(self.reading)
    return

  @Command(command="MEASure:VOLTage?")
  async def read_volts(self):
    self.read()
    print(self.volts)
    return

  @Command(command="MEASure:FIELd?")
  async def read_tesla(self):
    self.read()
    print(self.teslas)
    return

mag = Magnetometer()
mag.assign_adc(26)
mag.load_cal()

led = Pin("LED", Pin.OUT)

for i in range(3):
  led.value(1)
  sleep_ms(200)
  led.value(0)
  sleep_ms(200)

led.value(1)

while True:
  mag.run()
```